IOP Publishing Bioinspir. Biomim. 18 (2023) 041003 https://doi.org/10.1088/1748-3190/acddc1

Bioinspiration & Biomimetics

OPEN ACCESS

RECEIVED
22 March 2023

REVISED
8 June 2023

ACCEPTED FOR PUBLICATION
12 June 2023

PUBLISHED
28 June 2023

TOPICAL REVIEW

Biomimetic polymer fibers—function by design

Thomas Ebbinghaus[1], **Gregor Lang**[2,*] **and Thomas Scheibel**[1,3,4,5,6,*]

[1] Chair of Biomaterials, University of Bayreuth, Prof.-Rüdiger-Bormann-Str. 1, 95447 Bayreuth, Germany
[2] Department of Functional Materials in Medicine and Dentistry, University Hospital of Würzburg, Pleicherwall 2, 97070 Würzburg, Germany
[3] Bayreuth Center for Colloids and Interfaces (BZKG), University of Bayreuth, Universitätsstraße 30, 95447 Bayreuth, Germany
[4] Bavarian Polymer Institute (BPI), University of Bayreuth, Universitätsstraße 30, 95447 Bayreuth, Germany
[5] Bayreuth Center for Molecular Biosciences (BZMB), University of Bayreuth, Universitätsstraße 30, 95447 Bayreuth, Germany
[6] Bayreuth Center for Material Science (BayMAT), University of Bayreuth, Universitätsstraße 30, 95447 Bayreuth, Germany
[*] Authors to whom any correspondence should be addressed.

E-mail: thomas.scheibel@bm.uni-bayreuth.de and gregor.lang@uni-wuerzburg.de

Keywords: biomimicry, bio-inspiration, silk fibers, collagen fibers, tissue engineering, textiles, filters

Abstract

Biomimicry applies the fundamental principles of natural materials, processes, and structures to technological applications. This review presents the two strategies of biomimicry—bottom-up and top-down approaches, using biomimetic polymer fibers and suitable spinning techniques as examples. The bottom-up biomimicry approach helps to acquire fundamental knowledge on biological systems, which can then be leveraged for technological advancements. Within this context, we discuss the spinning of silk and collagen fibers due to their unique natural mechanical properties. To achieve successful biomimicry, it is imperative to carefully adjust the spinning solution and processing parameters. On the other hand, top-down biomimicry aims to solve technological problems by seeking solutions from natural role models. This approach will be illustrated using examples such as spider webs, animal hair, and tissue structures. To contextualize biomimicking approaches in practical applications, this review will give an overview of biomimetic filter technologies, textiles, and tissue engineering.

1. Introduction

Over hundreds of millions of years, highly complex strategies have evolved to tackle the survival challenges of organisms and to continuously adapt to dynamic environmental conditions in diverse ecosystems. Given that every living organism is constructed from materials, it is not surprising that complex organisms require highly advanced materials at all hierarchical levels. This includes a complex interplay of molecular structures of biomacromolecules and polymeric materials, mesostructured building blocks that incorporate gradients, anisotropy, and composite structures to construct tissues, organs, and in some cases even materials secreted externally for uses such as hunting or protecting offspring. Consequently, evolution influences not only materials but also processes, structures, and resulting functions (figure 1). The mimicry of nature's outstanding design concepts by mankind has a long tradition, thought to have originated thousands of years ago. Since the middle of the last century, the transfer of concepts from nature to technology has been called biomimicry, as introduced by Otto Schmitt in 1969. This term will be used in this context throughout the manuscript [1].

Biomimetic strategies can be applied either from a top-down or bottom-up perspective [2]. Both approaches are based on the hypothesis that nature offers solutions for a wide range of problems. Top-down processes begin by defining the problem and then seeking an analogy in nature that helps to solve it. Conversely, bottom-up processes are based on the fundamental research of biological systems. Knowledge of natural principles can then be transferred, as needed, to technical applications. Several biological principles have found their way into technological applications, among them are self-cleaning, high and dry adhesion, mechanical strength, hierarchical structures at the micro- and nanoscale, and thermal insulation [3].

In this review, the focus is on biological systems defined by their inherent polymeric materials, material processing, or material structures (figure 2). Bottom-up approaches aim to identify the underlying

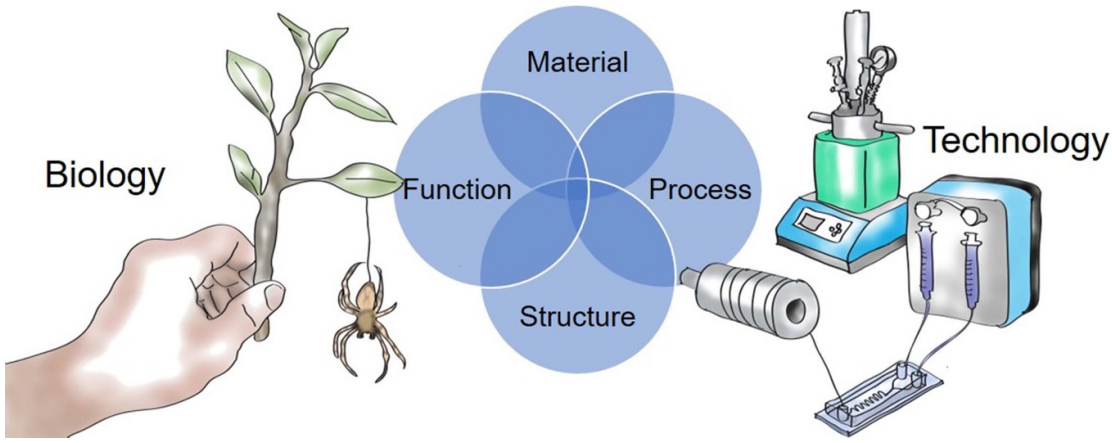

Figure 1. The concept of biomimicry: fundamental understanding of biological materials, processes, structures and functions leads to innovations in technology.

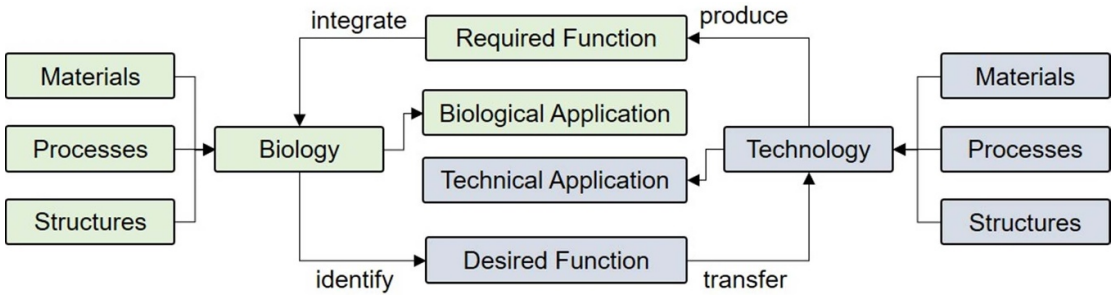

Figure 2. Schematic of strategy for biomimicry: biomimicry is used to enable both biological and technical applications. The identification and transfer of functions from biology leads to advancements in technology. Technology can produce required functions for biological in vivo applications.

mechanisms that allow the transfer of a desired function, first into a material and then into technological applications. On the other hand, advancements from technological approaches regarding materials, processes, and structures can also be introduced into biological systems to fulfill a required function. One prominent example is a medical implant. Medical implants must mimic natural functionalities and need to be successfully integrated into a biological environment. The iterative and contextual research from different disciplines in natural science and technology enables the development of innovative material concepts.

Here, we concentrate on biomimetic polymer fibers, highlighting the concepts derived from nature and how they can be emulated for technical applications. We also address the technical production of functional materials defined by biomimetic architecture. These materials are not only bioinspired but also intended for biological applications.

2. Bottom-up strategies for biomimetic fiber processing

Biopolymeric fibers are ubiquitous in nature, with prominent examples of high-performing biological fibers being silk, collagen, cellulose, and keratin [4]. Nevertheless, given that cellulose and keratin fibers are readily available from plants and animal hair, there is little motivation to artificially reproduce such fibers using a biomimetic bottom-up strategy. On the other hand, silk, and in particular spider silk, exhibits highly attractive properties such as mechanical stability, biocompatibility, and in some cases, resistance to microbial infestation [5]. Given that farming spiders on an industrial scale is not viable, there is considerable scientific interest in artificially producing these fibers, making them available for various applications. Furthermore, collagen fibers are highly attractive for regenerative medicine, and technical production routes that enable the creation of highly pure collagen-based fibers with reproducible quality could reduce the need for autografts and allografts. Both silk and collagen are made of biocompatible structural proteins that assemble into a hierarchically ordered fibrillar structure and, in this architecture, provide highly demanding mechanical properties. In light of the significance of these materials and their potential applications, the following section will focus on the processing of these two fibrous systems to yield biomimetic fibers.

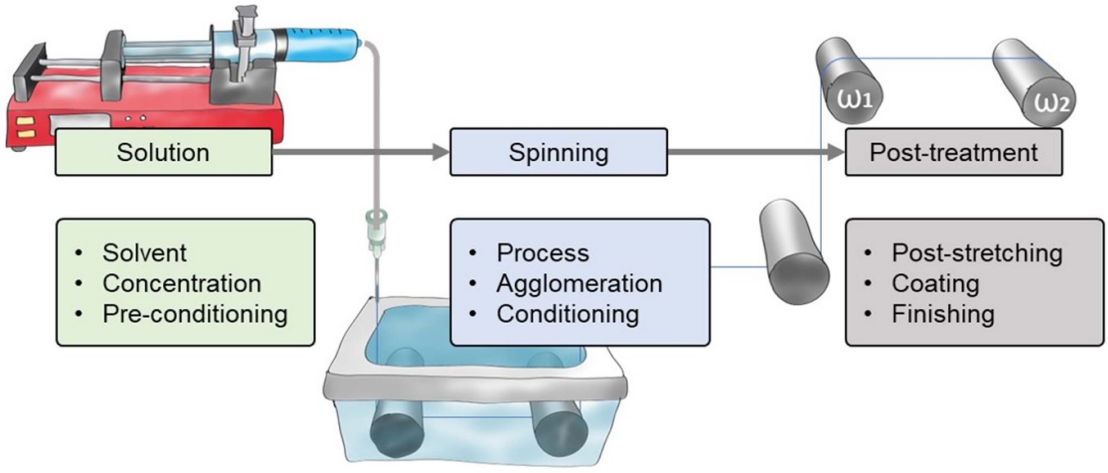

Figure 3. Different categories for biomimicry of natural spinning processes. The first category comprises primarily materials for the spinning solutions, the second the spinning process and conditions and the third the post-processing.

Biological fiber processing operates under physiological conditions, in an aqueous environment, and at moderate temperatures. These natural conditions must be somewhat emulated to allow for the assembly of organized hierarchical structures that result in superior mechanical properties. The development of nature-mimicking strategies may start with the solution, specifically the choice of material, solvent, concentration, or the preconditioning, such as pre-assembly of the underlying polymer. Furthermore, spinning and post-treatment conditions are essential within fiber processing strategies. The former encompasses the choice of spinning method, the mechanism of fiber solidification, and the spinning conditions. The latter covers processes like post-stretching, coating, and finishing to produce a fibrous product with the desired properties. Figure 3 provides an overview of the relevant aspects for mimicking the properties and functions of such fibers.

Considering that the melting temperature of most natural polymers exceeds their degradation temperature, melt processing is not applicable, and processing predominantly occurs from a solution. As for fiber production, the mechanism of solidification can either be based on coagulation, using a non-solvent as applied in wet-spinning and microfluidic spinning (figures 4(A) and (B)), or by drying, as in the case of dry-spinning and electrospinning (figures 4(C) and (D)).

Wet-spinning is a well-established solution-spinning technology used to produce continuous filaments from polymers. Due to its ease of scalability and economic efficiency, it is widely employed to produce textile fibers such as viscose, nylon, spandex, and acrylic fibers [6, 7]. In the wet-spinning process, the spinning solution is continuously extruded into a coagulation bath through a spinneret [8, 9]. The coagulation medium is a non-solvent for the polymer. The spinneret can have one or more orifices to obtain a single fiber or a multifilament. Upon immersion in the coagulation bath, a diffusive exchange leads to the solidification of the extruded polymer filament. During coagulation, the solvent diffuses out of the nascent fiber, while the non-solvent diffuses into the fiber. The filament is pulled out of the bath, for instance, with a winding unit. Between the bath and the winding unit, different steps of post-treatment can take place, such as washing, post-drawing, or heat treatment. The entire process is influenced by several parameters like the system of solvent and non-solvent determining miscibility and diffusion coefficients, process temperature, polymer concentration, and winding speed [10].

Microfluidic spinning is a technique that works with small volumes of solutions in a very confined space [11] and offers the ability to precisely control flow conditions within its microscale channels [12]. Microfluidic spinning is predominantly conducted using a core flow, formed by the polymer solution, and a sheath flow, which both stabilizes and elongates the core flow and can also be used to initiate fiber formation via anti-solvent-induced coagulation [13]. This technique is often employed for scientific purposes as it provides the capability to implement highly complex conditions, such as the combination of various sheath flows, the application of gland-like flow channel geometries, and microscopic *in-situ* observation via imaging through the transparent polydimethylsiloxane (PDMS) microfluidic chips. While microfluidic spinning is usually carried out as a special case of wet-spinning, it has also been shown to be applicable for dry-spinning.

Dry-Spinning is also a solution-spinning technology. However, in contrast to wet-spinning, solidification is not achieved through coagulation but via drying [14]. The formation of a fiber after extrusion is a consequence of solvent evaporation. Therefore,

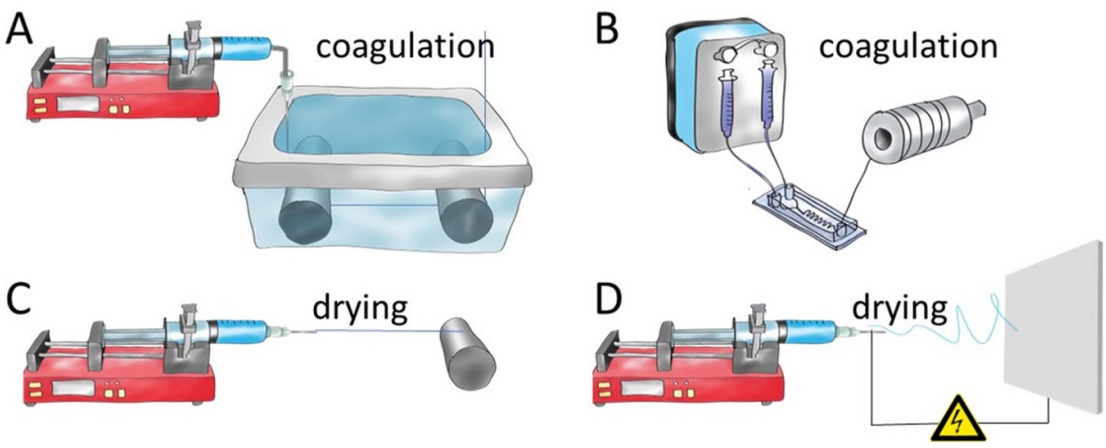

Figure 4. Schematic drawings of the major methods used for solution spinning: (A) wet-spinning, (B) microfluidic spinning, (C) dry-spinning and (D) electrospinning.

the used solvent must be volatile. The rate of evaporation can be improved by spinning into a heated evaporation chamber or hot air streams, as demonstrated, for example, with dry-spun polyimide fibers [15]. Subsequent to solidification, post-treatment, analogous to wet-spinning, can be carried out. For instance, regenerated silk was heat-stretched after dry-spinning [16]. Dry-spinning can also be combined with wet-spinning in a so-called dry-jet wet-spinning process, in which the jet is exposed to an air gap before being immersed in a coagulation bath. Shear forces and stretching induce molecular chain alignment, resulting in excellent mechanical properties [17]. This spinning technique was also successfully applied to fabricate strong fibers from natural polymers such as cellulose and lignin [18, 19]. Another dry-spinning technique is the pressurized gyration spinning process [20, 21]. The general setup consists of a cylinder fed with spinning solution and equipped with orifices or nozzles on the outer plane. The cylinder is connected to a motor to enable high rotating speeds and a gas supply to exert additional pressure on the solution. Due to centrifugal forces and the additionally applied gas pressure, fibers in the nano- to microscale can be extruded. The volatile solvent evaporates during the time of flight until the fibers reach a collector. In contrast to centrifugal spinning, which applies only centrifugal force to the spinning solution, the pressurized gyration process applies both centrifugal force and additional pressure.

Electrospinning can be used as both a melt and solution spinning technique to produce polymeric micro- and nanofibers [22, 23]. Electrospinning utilizes an electrostatic field to eject fibers from a spinning solution. The basic setup comprises a high-voltage supply, a spinneret, and a collector. The applied voltage is usually in the range of 5–30 kV [24]. The spinneret in a laboratory setup often consists of a syringe, filled with the spinning solution, equipped with a blunt metal needle, and mounted in a syringe pump [25]. The needle is connected to the voltage supply, and a grounded or oppositely charged collector, which can be a metal plate or a rotating drum, is placed at some distance from the needle (typically 10–30 cm). As a droplet of spinning dope is extruded from the needle, the electrostatic field induces charges at the droplet's surface, resulting in deformation into a so-called Taylor cone. As the repulsive forces of the accumulated charges and the Coulomb force of the external electrical field overcome the counteracting surface tension of the solution, a jet can be ejected from the tip of the Taylor cone [26]. On its way towards the collector, whipping occurs due to bending instabilities, and the jet is stretched and dries before reaching the collector. Finally, a solid fiber is deposited in the shape of a nonwoven mat (on a metal plate) or as an aligned fiber mat (on a fast-rotating drum) [27].

2.1. Mimicking the properties of silk fibers

Silk fibers provide an excellent example of a natural material displaying a unique combination of highly desirable properties such as mechanical strength (table 1), microbe-resistance (in some cases), biocompatibility, biodegradability, and non-immunogenicity. On the one hand, these properties make silk materials a perfect candidate for medical applications [28]. On the other hand, artificially reproducing such properties has proven to be highly challenging. Compared to, for instance, a melt-spun plastic fiber, silk fibers are built up in a much more complex hierarchical structure that is not solely based on the underlying silk proteins, but is also highly dependent on the processing conditions and technique. Strikingly, this complexity is further emphasized when comparing the silk spinning mechanisms of spiders and silkworms—two completely different species that have developed nearly identical highly complex spinning mechanisms, including silk gland geometries, highly concentrated aqueous spinning solutions, ion exchanges, pH drops, water resorption, and shear forces [29–31]. Silk fiber formation

Table 1. Overview of mechanical properties of silks and other materials (* 100% relative humidity) [39].

Material	Strength (GPa)	Extensibility (%)	Toughness (MJm^{-3})
Araneus major ampullate silk	1.1	27	160
Bombyx mori cocoon silk	0.6	18	70
Nylon fiber	0.95	18	80
Kevlar 49 fiber	3.6	2.7	50
Carbon fiber	4	1.3	25
Wool*	0.2	50	60
Synthetic rubber	0.05	850	100
Elastin	0.002	150	2

can be characterized as a liquid-to-solid phase transition, which is induced as the highly concentrated (∼50%w/v) spinning dope passes the tapered spinning duct [32]. Due to the tapered form of the duct, shear stress and elongational flow increase, which are assumed to promote the alignment of the proteins and, ultimately, anisotropic fibril formation. Simultaneous dehydration and ion exchanges occur, where sodium and chloride levels are reduced, while phosphate and potassium concentrations increase [33]. The replacement of the more chaotropic ions with more kosmotropic ones is thought to promote the structural arrangement of the proteins by exposing the hydrophobic dimeric areas of the carboxy-terminal domains (CTDs) in a parallel conformation, which are crucial for spider silk assembly. The decrease in pH value (spider major ampullate gland: 7.2–5.7 and silkworm: 7.1–6.2) [33, 34] induces a conformational change in the CTDs. In addition, it triggers the antiparallel dimerization of an amino-TD (NTD) in the case of spider silk. Shear forces on the spinning dope originate from the pulling of the thread by the spider's legs or, alternatively, the silkworm's head. The final mechanical properties of silk fibers are, therefore, a consequence of (a) the molecular architecture of the silk proteins, (b) the intermolecular assembly of the proteins, and (c) their processing. Especially crystalline domains formed by beta-sheet structures account for the mechanical strength and stiffness of the fibers.

Unlike silkworms, most spiders cannot be domesticated due to their territorial and cannibalistic nature [35]. Thus, an alternative route to access this material has been developed, the recombinant production and processing of spider silk proteins. Nonetheless, bottom-up biomimicry of the natural silk spinning process is required to reproduce the desired properties, and research to tackle this challenging task has been ongoing for decades [35–38].

2.1.1. Regenerated B. mori silk

Biomimicry begins with the preparation of spinning solutions. In the case of silkworm (*B. mori*) silk, native cocoon silk must be degummed to obtain regenerated silk fibroin. Degumming is carried out to remove glue-like sericin proteins that cover the fibroin double filaments. It is typically performed by boiling in an alkaline solution, which can result in hydrolytic molecular degradation [40, 41]. Therefore, alternative strategies such as enzymatic degradation of sericins have been studied with the goal of maintaining high molecular weight fibroin upon degumming [42–44]. Moreover, spinning conditions and post-treatment significantly impact the resulting properties of regenerated fibroin fibers. Wei *et al* reported capillary dry-spinning of regenerated silkworm fibroin (RSF) [45]. They used 44–48 wt% aqueous solutions, which were dry spun into air at low humidity. The solvent evaporated within a 10 cm distance from the winding unit, and fibers were dried afterward for 24 h, followed by post-drawing in 80% ethanol. This approach yielded fibers with an average breaking strength of 298 MPa and diameters of around 15 μm. Regarding mimicking natural spinning conditions and analyzing their impact on fiber properties, dopes at a pH between 5.2 and 6.9, as observed in nature, were tested and yielded excellent spinnability. In contrast, lower pH values and the addition of different metal ions (magnesium and potassium) disrupted the continuous spinning process. Among other reasons, this could be a consequence of rapid gelation. Jin *et al* further developed this setup [46]. Their spinning solution had a concentration of 40–60 wt%, and calcium chloride ($CaCl_2$) was added to adjust the calcium concentration to 0.3 M. At these conditions and with applied post-stretching in diluted ethanol, the breaking strength could be increased to 357.3 MPa. Additionally, the beta-sheet ratio of post-drawn fibers was determined to be 47%, thus increasing compared to the spinning parameters used by Wei *et al*. This value is close to the beta-sheet content of 50% in degummed cocoon silk. The authors therefore concluded that a pH drop can be neglected. Peng *et al* transferred these spinning conditions to a microfluidic setup to investigate the effect of humidity on fiber structure and properties [47]. The microfluidic chip mimicked the natural aspect of a tapered spinning duct. They used a fibroin concentration between 38 and 47 wt%. The relative humidity was varied between 40 and 50%. It was observed that fibers spun at 40% relative humidity were consistently thinner than those spun at 50%.

This could be a result of differing rates of solidification. The diameters were in the range of 5–10 μm. The lower humidity affected the secondary structure content as well and increased the amount of beta-sheets. The content of beta-sheets approached, and even exceeded, that of beta-sheet structures in degummed silk, depending on the fibroin concentration in the spinning solutions. However, once again, the tensile stress of the fibers could be increased up to 541 MPa.

Luo *et al* used a microfluidic setup, including a single channel microfluidic chip, to mimic the tapered shape of a spider's spinning duct [48]. The chips were fabricated using PDMS. The width of the channel decreased exponentially from the inlet of 2000 μm to the outlet of 100 or 250 μm. The height of the channel was kept constant at 85 μm The reduction in width generated increasing shear forces and elongational flow, promoting the alignment of the silk fibroins in the spinning solution. Bombyx mori silk fibroin, regenerated at 50 wt% in aqueous buffer, was dry-spun, reeled in air, and post-drawn in 80 vol% ethanol. The authors fabricated two types of fibers: a monofilament with a diameter of around 12 μm spun from the 250 μm outlet, and a multifilament with a diameter of 2 μm spun from the 100 μm outlet. The latter mimics the hierarchical buildup of spider dragline and silkworm silk, exhibiting a multifibrillar microstructure. Mechanical testing of the spun filaments showed superior performance of the post-drawn multifilament silk fibers compared to the monofilament and degummed cocoon silk, with a breaking stress of 614 MPa and a breaking strain of 27%. These values closely match the natural blueprint (table 1). Post-drawing was shown to increase the amount of beta-sheet crystals, accounting for the achieved mechanical strength. The post-drawn multifilament demonstrated the highest content of beta-sheets compared to both the other samples and the degummed silk fibers. Li *et al* took a further step to approach the natural silk spinning process in 2017 [49]. In addition to introducing shear stress on the spinning solution, they incorporated ion gradients into a sheath flow microfluidic setup. These ion gradients were achieved by adding potassium and hydrochloric acid (KCl and HCl) to a PEO sheath flow and $CaCl_2$ to an 8%w/v silk solution. After spinning, the samples were sequentially incubated in methanol and water, without post-drawing, and then dried. The authors investigated the impact of these ions on the secondary structure content and the mechanical properties of the fibers. The addition of metal ion gradients seemed to influence the secondary structure, as an increase in beta-sheets was observed, a phenomenon that did not occur when applying shear stress alone. Mechanical properties showed an increase in ultimate tensile strength and extensibility upon introducing the ion gradient and combining it with the sheath flow. However, despite closely mimicking the natural setup, the maximum tensile strength of the fibers achieved was 47.28 MPa with a respective extensibility of 12%, significantly below the strength of natural silk fibers. To overcome this issue, the authors proposed to increase the effective shear stress by, for instance, increasing the concentration of the silk solution. It must be noted that this study abstained from post-drawing, a technique typically used to enhance the tensile strength of fibers and also applied in nature.

Satoh *et al* dry-spun RSF aiming to mimic a fiber with properties like that in the natural cocoon silk [16]. They dissolved fibroin in 1,1,1,3,3,3-hexafluoro-2-propanol (HFIP), a highly volatile organic solvent, and added the ionic liquid 1-hexyl-3-methyl-imidazolium chloride (HMIM-Cl) to the solution. The spinning solution was spun into air and guided onto a first winding unit after 100 cm. The filament was then dried under vacuum for more than 5 h. The fibers were subsequently heat-stretched, immersed in methanol to remove the ionic liquid, and dried again under vacuum. The use of a two-solvent system, the volatile HFIP and the non-volatile HMIM-Cl, inhibited overly rapid solidification of the fiber. Consequently, a smooth surface without pores and a core without voids could be achieved. However, the cross section of the spun fibers was belt-like instead of circular, which was attributed to the plasticization through HMIM-Cl. Energy-dispersive x-ray spectroscopy was used to demonstrate the complete removal of the ionic liquid after washing. The highest recorded yield strength of the fibers was 159.9 MPa, with a corresponding breaking strain of 31.5%. Thus, the achieved toughness was lower compared to the natural blueprint, but the use of the ionic liquid might be a strategy to achieve compact fibers in the future.

Magaz *et al* employed solution blow-spinning of regenerated silk fibroin in aqueous- and formic acid-based (FA) solutions, combined with an inline vapor post-treatment [50]. This technique allowed the fabrication of random and aligned nonwoven meshes, with fiber diameters in the range of 260–910 nm. The resulting ultimate tensile strength varied significantly between fibers spun from aqueous or FA solutions. The former led to an ultimate tensile strength of 0.3 MPa, while the latter resulted in 3.5 MPa. By using a coaxial nozzle, the authors tried to mimic natural fiber formation aspects like pH drop and substitution of metal ions. However, the fibers produced were not analyzed with respect to their mechanical properties. Examination of the secondary structure content showed an increased amount of beta sheets compared to untreated fibers. This observation could be due to the fact that self-assembly was induced, which would reflect an approach to integrate biomimetic aspects into conventional solution blow spinning.

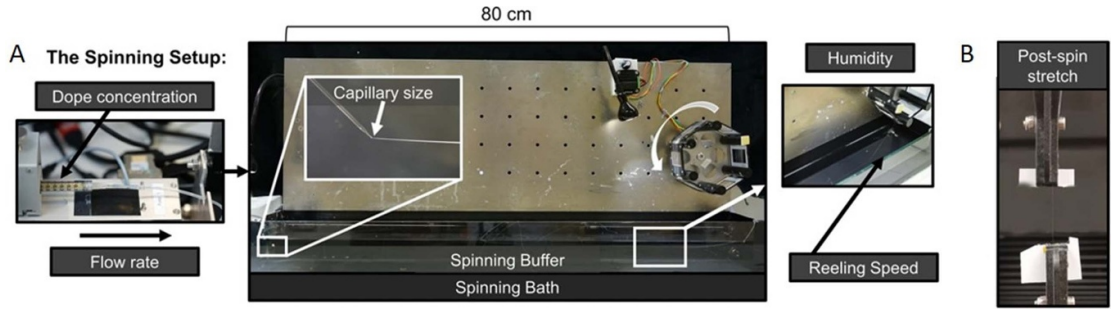

Figure 5. Wet-spinning setup by Schmuck *et al*. Reproduced from [54]. CC BY 4.0.: The spinning solution is transferred in a syringe and mounted on a syringe pump (left). The solution is extruded in an aqueous buffer coagulation bath and reeled with a winding unit (middle). The fibers are post-stretched in air (right). Licensed under CC BY 4.0.

2.1.2. Recombinant spider silk

As described above, spider silk cannot be efficiently obtained from living spiders, but recombinant spider silk proteins (spidroins) present a highly interesting alternative [35–37]. FA and HFIP, often used as solvents for spidroin spinning, result in pronounced denaturation of the protein secondary structure, thereby inhibiting natural pre-assembly mechanisms like micelle formation [51]. Replacing these organic solvents with aqueous solvent systems is a fundamental prerequisite for a biomimetic setting, but this approach relies on proteins that are soluble in aqueous buffers. Andersson *et al* designed a recombinant spidroin called NT2RepCT based on a repetitive domain of *E. australis*, flanked by non-repetitive NTDs and CTDs, based on *A. ventricosus* sequences [52]. Both TDs are highly soluble and pH-responsive. The protein could be concentrated between 10%w/v and 50%w/v in aqueous spinning solutions. These concentrations were achieved by centrifugal filtration of the purified protein. The proteins formed micelles in solution, which elongated upon the introduction of shear from a pulled glass capillary with a tip diameter of 10–30 μm, and these solutions were spun into aqueous coagulation baths. The pH of the coagulation bath had a significant impact on fiber formation. Continuous fibers could only be spun in a pH range from 3.0 to 5.5. Outside that range, fiber fragments or no fiber formation was observed. Greco *et al* further wet-spun a 30%w/v aqueous solution of NT2RepCT spidroin into an aqueous buffer at a pH of 5.0 [53]. Incubating the fibers for more than five hours in the coagulation bath improved both the mechanical properties and water insolubility. Significant morphological changes due to this treatment were not observed. The improvement is attributable to an increased beta sheet content of the fibers, yielding a tensile strength of 70 MPa with a corresponding strain at break of 30%. Schmuck *et al* used the same spidroin and conducted a comprehensive study on the impact of various spinning parameters on the mechanical properties (figure 5) [54]. According to their studies, the reeling speed and the post-drawing are the most important parameters to improve the mechanical performance of the wet-spun fibers. With their optimal setup of spinning conditions, they achieved a fiber toughness of 129 MJm^{-3}. This toughness is around two and a half times higher than that of Kevlar. They also showed that further post-stretching to 80% increased the fiber strength while decreasing the toughness. These results indicate the possibility of adjusting the properties of the fibers to some extent to meet application requirements.

In 2022, Arndt *et al* published a study in which NT2RepCT was modified to produce fibers with a toughness equivalent to that of natural dragline silk [55]. As discussed previously, beta sheets are the structural components responsible for the mechanical strength of silk. Consequently, they designed a spidroin based on NT2RepCT, which contains more amino acid motifs capable of forming beta sheets. The fibers were spun as reported previously, but were only minimally stretched during the reeling from the coagulation bath. Fourier-transform infrared (FTIR) spectroscopy revealed that fibers spun from such modified protein variants indeed showed an increased amount of beta sheets. Tensile testing indicated that one of the variants exhibited an increased toughness of 146 MJm^{-3}, which is comparable to that of native dragline silk.

In another study, biomimetic silk fibers with the same toughness as native dragline silk were produced by Heidebrecht *et al* in 2015 [56]. Here, the protein used was based on the sequence of a major ampullate dragline fibroin of *A. diadematus* (ADF3). Eight variants differing in length and the presence or absence of TDs were analyzed. The spinning solution was wet-spun into a mixture of isopropanol and water as a coagulation medium. After solidification, the fibers were post-stretched up to 600% to induce the structural conversion to beta sheets and to further align the spidroins. The study of the mechanical performance of the fibers revealed that biomimetic preparation of the spinning dope via dialysis against sodium

phosphate buffer allowed self-assembly of proteins with TDs. These phase-separated, highly concentrated biomimetic spinning dopes yielded fibers with significantly increased toughness. The variant with both an NTD and CTD even displayed a toughness of 189 MJm^{-3}, outperforming the toughness of the natural counterpart. In a detailed investigation using dynamic light scattering, light microscopy, and nuclear magnetic resonance (NMR), Stengel *et al* elucidated that this biomimetic dope preparation induces differences at the molecular structural level [57]. The results show that during preparation using phosphate buffer, self-assembly continuously advances over time until a liquid-liquid phase separation, which is not the case for dopes prepared by conventional dialysis against poly-ethylene-glycol. Slight differences in both the dopes and the spun fibers were observed using NMR. Concerning the dope, a higher degree of assembly in case of the biomimetic dope and differences in the conformation of tyrosine residues were noticed. Solid-state NMR did not show structural disagreements in the beta-sheet regions of the fibers, but in the non-beta-sheet domains in the form of different packaging of tyrosine aromatic rings. These differences seem to be responsible for the significant improvement of the mechanical properties. Another step to get closer to the natural blueprint of *A. diadematus* dragline silk was taken by Saric *et al* [58]. *A. diadematus* dragline silk is a composite fiber and consists of at least the two major ampullate 2 spidroins, ADF3, and ADF4 [37]. In contrast to most approaches using only one spidroin, Saric *et al* used co-expression of engineered ADF3 and 4 (eADF3, eADF4) to spin composite silk fibers using microfluidic wet-spinning with a sheath flow of phosphate buffer and subsequent post-drawing up to 400%. As described before, spin dopes were produced by dialysis against phosphate buffer, which enabled dimerization and self-assembly through the CTDs. The wet-spun fibers were mechanically characterized, showing a tensile strength of 834 MPa and an extensibility of 32%, which exceeds all previously presented properties. The fibers spun with co-expressed protein were also compared to an *in vitro* mixture of the two spidroins. Their mechanical performance was significantly lower, exhibiting a strength of 614 MPa, which could be a consequence of reduced molecular alignment due to the preparation method. In a recently published approach, Saric and Scheibel used the amino acid sequences of eADF3 and eADF4 to generate a new spidroin variant containing parts of both sequences and TDs [59]. The spinning solution, fiber spinning, and post-treatment were conducted as described before. The new variant was subjected to extensive characterization. Wet-spun fibers were analyzed regarding their mechanical properties and displayed a tensile strength of 419 MPa. The reduced strength compared to the results presented before could, among other reasons, be due to the reduced molecular weight of the newly designed variant. However, the work of Saric *et al* demonstrates the immense potential of silk fibers when closely mimicking the key aspects of the natural process.

Lu *et al* used a microfluidic chip to mimic the shape of a spider's major ampullate gland and spinning duct [60]. In addition to the biomimetic shear force-inducing spinning setup, they incorporated cellulose nanofibers (CNFs) to reinforce the resulting fibers. To do this, they blended a 45 wt% aqueous RSF solution with different ratios of CNFs before dry-spinning. Their microfluidic chip was composed of three segments responsible for storage, elongation, and shear. The width of the channel decreased from 4 mm to 244 μm from the inlet to the outlet, while the depth was kept constant at 150 μm. After dry-spinning, the fibers were post-stretched in 80 vol% ethanol before drying. In the case of a ratio of 1/1000 between CNFs and silk (RSF/CNF 1), they achieved fiber diameters in the range of 8 μm. Mechanical testing of the fibers indicated an improvement of the tensile strength due to the CNFs. RSF/CNF 1 fibers displayed a tensile strength of 487 MPa with a breaking strain of 16%. This study highlights the possibility of exceeding the mechanical properties of the natural model by combining biomimicry with well-known reinforcement strategies.

Jao *et al* used an advanced electrospinning (e-spinning) setup to mimic the hierarchical structure of native silk in an aligned e-spun mat [61]. The molecular and hierarchical buildup of silk is the reason for its excellent mechanical toughness, which outcompetes many synthetic fibers [62]. The setup of Jao *et al* consisted of a conventional e-spinning setup, which was extended with two parallel track-drawing devices (figure 6). These devices were mounted to the left and right of the propagation direction of the solidifying jet. When RSF-fibers were spun, they stuck onto the surface of the top of the rotation drawers. During the rotation, the fibers were transported downwards. Meanwhile, they became aligned and were stretched until they were deposited on a collector at the bottom of the setup. The degree of stretching was defined by the geometry of the setup. Consequently, post-drawing, as applied by both spiders and silkworms in nature, was mimicked in the described setup. It induced further alignment of protein chains inside the fibers and increased the number of crystalline beta-sheets inside the protein. Using FTIR spectroscopy, the secondary structure was probed and revealed an increasing number of beta-sheets with increasing draw ratio. Accordingly, by increasing the draw ratio, the ultimate strength of the fibrous mat was increased up to 640 MPa, while the maximal elongation decreased.

In conclusion, it can be said that biomimetic strategies consistently result in superior mechanical properties when processing silk fibers. Table 2 provides an overview of the examples discussed,

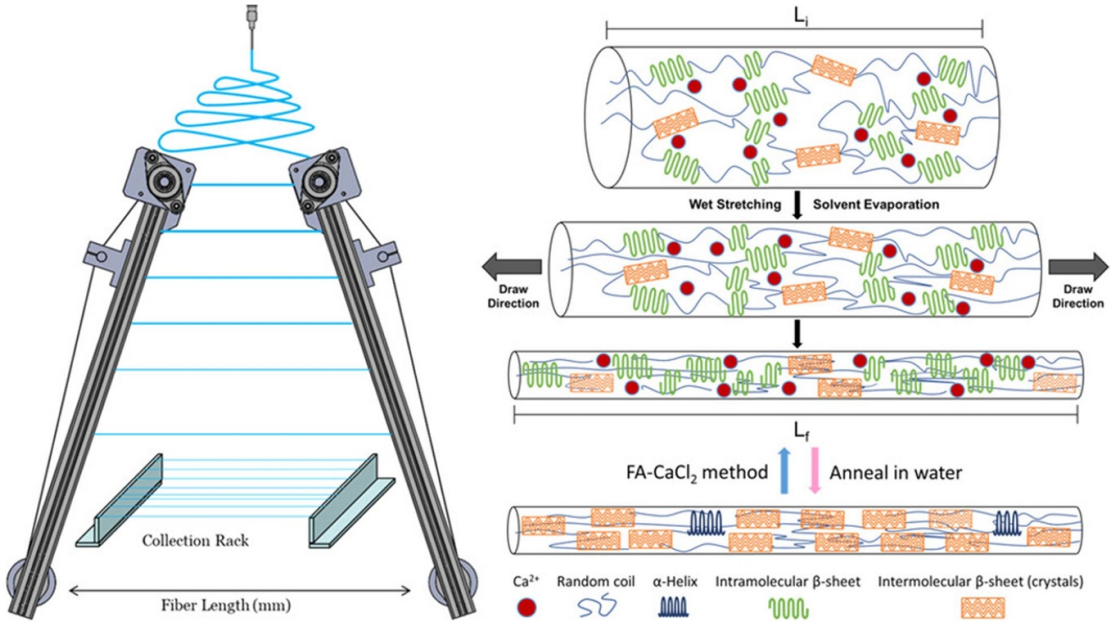

Figure 6. Schematic of track drawing setup, which combines electrospinning and post-drawing of the spun nanofibers (left). The post-drawing and post-treatment induce structural changes in the fibers increasing Young's modulus and ultimate tensile strength (rights). Reprinted with permission from [61]. Copyright 2021 American Chemical Society.

summarizing the most relevant aspects regarding materials and solution, processing methods and post-treatment, as well as the characteristic fiber properties in terms of diameter and mechanics. Furthermore, the respective approaches were categorized according to their degree of biomimicry (figure 7(A)). This means that approaches, where only the solutions were biomimetic (aqueous and highly concentrated), are depicted with one point (green), and approaches where, for instance, biomimetic spinning (blue point) and post-treatment (grey point) were performed in addition are categorized with three points. By correlating these three categories with the toughness of the resulting fibers, the aforementioned effect of promoting the mechanical strength of silk materials by applying biomimetic principles can be well visualized since there is a clear trend towards enhanced toughness with a higher degree of biomimicry. In this context, the spinning dope concentration seems to play a crucial role, as it has been shown that there is a clear trend towards high strength when concentrations approach the values of the natural spinning dopes of approximately 50%w/v (figure 7(B)).

2.2. Mimicking the properties of collagen fibers

Collagen is a structural protein that is abundant in the native tissue of humans and animals. Collagen is translated inside animal cells, where it forms triple-helices before being secreted into the extracellular matrix (ECM) to form fibrils, beaded filaments, anchoring fibrils, and networks [63]. There are various types of collagen, among which types I, II, III, and VI are categorized as fibril-forming collagens [64]. Depending on the specific requirements of the tissue, the diameters of assembled collagen fibrils can range from ∼16 nm (in cartilage) up to more than 250 nm (in tendon) [65]. Consequently, collagen fibrils and fibers are not actually spun in terms of a spinning process such as conducted by spiders and silkworms, but self-assemble. The fibrillary, hierarchical structure of collagen gives native tissue its properties like mechanical stability and elasticity, as well as porosity and transparency (as in the cornea) [66] The biomimicry of collagen-based fibers, with structural and mechanical properties comparable to the natural blueprint, is highly relevant in the field of tissue engineering and even considered for textile fibers. The following section will focus on collagen-based fibers produced via spinning technologies and with respect to mechanical properties. An overview of the selected examples is given in table 3.

Spinning of collagen fibers usually relies on denaturing solvents like HFIP, HCl, 2,2,2 trifluoroethanol (TFE), acetic and trifluoroacetic acid (TFA) [66]. These solvents contrast with the physiologically aqueous environment in which collagen is synthesized and secreted. Upon isolation of collagen from animal sources and processing of extracted collagen, the native protein architecture is lost [67]. Therefore, biomimetic research in this field addresses the use of naturally abundant collagen with the aim to achieve mechanical properties comparable to the natural counterpart and to generate fibers for medical applications, for example, tissue regeneration. Haynl *et al* spun collagen fibers using a microfluidic setup [68]. In the microfluidic chip, the spinning solution, collagen in acetic acid (pH 3), was surrounded by a sheath flow of buffer solution (pH 8). The sheath

Table 2. Overview of publications on biomimetic silk processing (*RSF: regenerated silk fibroin, **HMIM-Cl: 1-hexyl-3-methyl-imidazolium chloride, ***HFIP: 1,1,1,3,3,3-hexafluoro-2-propanol, ****FA: formic acid) .

Author, Year	Material	Solution	Processing Method	Post-treatment	Diameter	Mechanical Properties
Wei *et al* 2011 [45]	RSF*	44–48 wt% aqueous	Dry-spinning	Post-stretching in 80 vol% ethanol	14 ± 1 μm	Strength of 298 ± 61 MPa, strain 16%
Jin *et al* 2013 [46]	RSF	40–60 wt% aqueous + $CaCl_2$	Dry-spinning	Post-stretching in 80 vol% ethanol	6.3 ± 2.3 μm	Strength 357.3 ± 84.3 MPa, strain 34.1 ± 8.1%
Peng *et al* 2015 [47]	RSF	38–47 wt% aqueous	Microfluidic dry-spinning, biomimetic geometry	Post-stretching in 80 vol% ethanol	9.0 ± 1.3 μm	Strength 541 ± 26.1 MPa, strain 19.3 ± 4.8%
Luo *et al* 2014 [48]	RSF	50 wt% aqueous	Microfluidic dry-spinning, biomimetic geometry	Post-stretching in 80 vol% ethanol	2 μm (multifilament)	Strength 614 MPa, strain 27%
Li *et al* 2017 [49]	RSF	8.3% (w/v) aqueous	Microfluidic dry-spinning, biomimetic geometry, and ion gradients	Incubation in methanol	4–10 μm	Strength 47.28 ± 15.59 MPa, strain 12 ± 1.5%, toughness 29.29 ± 9.86 kJm^{-3}
Satoh *et al* 2022 [16]	RSF	RSF:HMIM-Cl**:HFIP*** = 15:3.75:81.25 (w/w/w)	Dry-spinning	Heat-stretching	—	Strength 159.9 MPa, strain 31.5%, toughness 43.2 MJm^{-3}
Magaz *et al* 2018 [50]	RSF	12% (w/v) FA	Blow-spinning	Inline vapor post-treatment	290 ± 60 nm	Strength 3.5 ± 0.7 MPa, strain 0.46 ± 0.10%, toughness 0.05 ± 0.01 MJm^{-3}
Andersson *et al* 2017 [52]	Recomb. spider silk (*E. australis*)	10%–50% (w/v) aqueous	Wet-spinning into 500 mM sodium acetate buffer and 200 mM NaCl (pH 5) bath	—	12 ± 2 μm	Strength 162 ± 8 MPa, strain 37 ± 5%, toughness 45 ± 7 MJm^{-3}
Greco *et al* 2020 [53]	Recomb. spider silk (*E. australis*)	30% (w/v) aqueous	Wet-spinning into aqueous buffer at pH 5	Incubation in spinning buffer	15 ± 7 μm	Strength 80 ± 64 MPa, strain 37 ± 56%, toughness 40 ± 70 MJm^{-3}
Schmuck *et al* 2022 [54]	Recomb. spider silk (*E. australis*)	10%–45% (w/v) aqueous	Wet-spinning into aqueous buffers	Post-stretching in air (20-80%)	6.6 ± 1.4 μm	Strength 261 ± 77 MPa, strain 32 ± 8%, toughness 68 ± 27 MJm^{-3}

(Continued.)

Table 2. (Continued.)

Author, Year	Material	Solution	Processing Method	Post-treatment	Diameter	Mechanical Properties
Arndt *et al* 2022 [55]	Recomb. spider silk (*E. australis*)	20%–40% (w/v) aqueous	Wet-spinning into aqueous buffer at pH 5	Minimal post-stretching	4.16 ± 0.78 μm	Strength 132 ± 32 MPa, strain 160 ± 37%, toughness 146 ± 42 MJm^{-3}
Heidebrecht *et al* 2015 [56]	Recomb. spider silk (*A. diadematus*)	10% (w/v) aqueous buffer	Wet-spinning into diluted isopropanol	Post-stretching in diluted isopropanol	27 ± 10 μm	Strength 370 ± 59 MPa, strain 110 ± 25%, toughness 189 ± 33 MJm^{-3}
Saric *et al* 2021 [58]	Recomb. spider silk (*A. diadematus*)	10%–15% (w/v) aqueous buffer	Microfluidic wet-spinning into phosphate buffer	Post-stretching in diluted isopropanol	27 ± 1 μm	Strength 834 ± 34 MPa, strain 32 ± 1%, toughness 143 ± 6 MJm^{-3}
Saric and Scheibel 2023 [59]	Recomb. spider silk (*A. diadematus*)	10%–15% (w/v) aqueous buffer	Microfluidic wet-spinning into phosphate buffer	Post-stretching in diluted isopropanol	18 ± 4 μm	Strength 419 ± 173 MPa, strain 24 ± 2%, toughness 61 ± 25 MJm^{-3}
Lu *et al* 2019 [60]	RSF & cellulose nanofibers	45 wt% aqueous	Microfluidic dry-spinning, biomimetic geometry	Post-stretching in 80 vol% ethanol	7.9 ± 2.0 μm	Strength 486.9 ± 106.6 MPa, strain 15.8 ± 4.7%
Jao *et al* 2021 [61]	RSF	15% (w/v) in FA**** and 4% (w/w) $CaCl_2$	Aligned electrospinning	Post-stretching in air	501.58 ± 58.83 nm	Strength 640 MPa, strain 28%

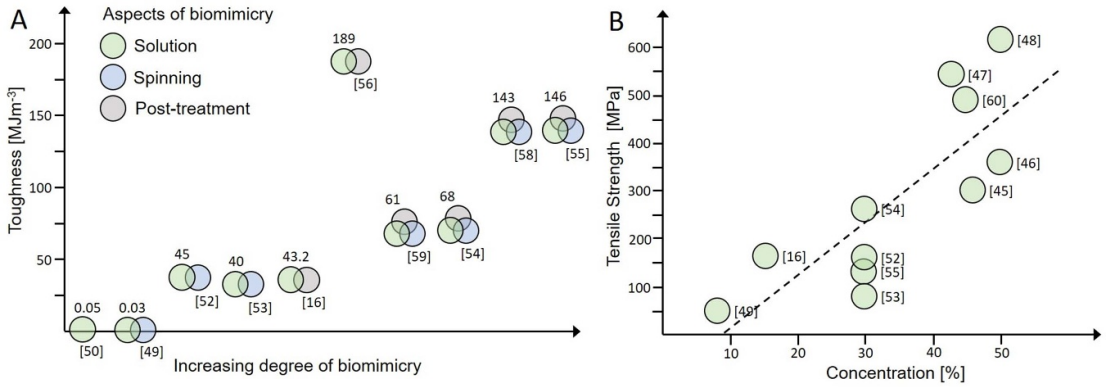

Figure 7. (A) Color-coded diagram of reported silk fiber toughness with respect to degree of biomimicry upon processing. The publications are rated regarding the afore described categories of biomimicry: solution, spinning and post-treatment. (B) Reported tensile strength plotted over respective concentration of the spinning solution. Dashed line represents linear trendline. References in brackets respectively.

flow neutralized the spinning solution, inducing fibril formation and increased alignment of the proteins. The fibers were pulled through a water bath for washing and finally wound up. The reeling of the filament was used to post-draw the fibers. With this setup, a minimum fiber diameter of 3 μm was realized. The resulting fiber diameter could be adjusted by tuning the flow rates of both buffer and spinning solution. Importantly, in contrast to the natural counterpart, this technique allowed the production of continuous collagen fibers. Mechanical characterization revealed a strength of 383 MPa and an extensibility of 25%. Fiber toughness was calculated to be 52.9 MJm^{-3}. The achieved elastic modulus and tensile strength exceeded the mechanical properties of tendons and all other man-made collagen fibers (table 3) [69, 70].

In contrast to microfluidic spinning, wet-spinning of extracted collagen often yields fibers with poor mechanical strength and water solubility, which makes pre- or post-treatment strategies necessary [66]. Therefore, artificial collagen fibers are often crosslinked to enhance their stability against wet conditions and improve their mechanical performance. Dasgupta *et al* published an extensive study comparing different crosslinkers and the resulting fiber properties [71]. They used a microfluidic setup to wet-spin collagen fibers. The spinning solution was fabricated with acetic or hydrochloric acid and extruded via a coaxial setup with a sheath flow of phosphate buffer into a coagulation bath of 20% ethanol. After drying, the fibers were crosslinked using more than 50 different approaches and analyzed using wet-tensile testing. Glyoxal-crosslinked collagen fibers exhibited an ultimate tensile strength of 299 MPa with a corresponding breaking strain of 9.5%. The fibers were further subjected to long-term stability and biocompatibility tests. Tronci *et al* investigated the impact of the molecular weight of two collagen-derived polypeptides on the resulting fiber properties [72]. They used gelatin and hydrolyzed fish collagen. The spinning solutions were prepared from 3% to 40% (w/v) collagen in either 2,2,2-TFE or dimethyl sulfoxide (DMSO). The spinning solution was extruded into a coagulation bath of ethanol or acetone and dried without further post-treatment. The fibers were then crosslinked using different methods. The authors showed that the resulting fiber diameter depends on the polymer, solvent, concentration, and coagulation medium. The diameters ranged from approximately 120 to 460 μm. The mechanical properties were affected by the spinning conditions and additionally by the method of crosslinking. Fibers spun from gelatin and crosslinked using 1,3-phenylenediacetic acid exhibited a maximum tensile stress of 65 MPa with a respective strain at break of 9% and Young's modulus of 726 MPa. Tonndorf *et al* examined the possibility of a non-toxic riboflavin-induced (RF) photo-crosslinking of collagen fibers, which is an important step regarding possible medical applications [73]. The spinning solution was prepared using acetic acid. The solution was wet-spun through a coaxial setup with a wet spinning buffer as a sheath flow into a bath filled with the same buffer. Subsequently, the fiber was drawn through a bath of 50 wt% ethanol and a third bath for the crosslinking of the fibers. The photo-induced crosslinking with RF was compared to that of the often-applied crosslinking agent glutaraldehyde (GA). Crosslinking with both methods led to collagen filaments that could be handled and mechanically tested in the wet state. However, GA-crosslinked fibers exhibited a tensile strength of 4.7 cN/tex, whereas the RF-crosslinked fibers only showed a strength of 1 cN/tex. Cell culture tests revealed improved cytocompatibility for RF photo-crosslinked collagen fibers compared to GA-crosslinked fibers. Yaari *et al* reported the wet-spinning and crosslinking of human recombinant collagen with the aim of application in regenerative medicine and tissue engineering [74]. Here, the concentrated spinning solution was prepared by dialysis

Table 3. Overview of publications on collagen fiber spinning (*TFE: 2,2,2-trifluoroethanol).

Author, Year	Collagen	Solvent	Processing Method	Post-treatment	Diameter	Mechanical Properties
Haynl *et al* 2016 [68]	Collagen type I	Acetic acid	Microfluidic wet-spinning into water	Post-drawing while reeling	3.7 ± 1.2 μm	Strength of 383 ± 85 MPa, strain 25.0 ± 3.7%, toughness 52.9 MJm^{-3}
Dasgupta *et al* 2021 [71]	Telo-, atelo-, methacrylated collagen	HCl, acetic acid	Microfluidic wet-spinning into 20 vol% ethanol	Crosslinking	34.1 ± 2 μm (width of untreated fiber)	Strength of 299 MPa, strain 9.5%
Tronci *et al* 2015 [72]	Fish collagen, gelatin	TFE*	Wet-spinning into ethanol/acetone	Crosslinking	120–460 μm	65 ± 12 MPa with a respective strain at break of 9 ± 1%
Tonndorf *et al* 2019 [73]	Calf skin collagen type I/III	Acetic acid	Wet-spinning into buffer	Crosslinking	52–114 μm	Strength of 4.7 cN/tex
Yaari *et al* 2016 [74]	Recombinant human collagen	HCl	Wet-spinning into PBS	Postdrawing, Crosslinking	10–35 μm	Strength of 151 MPa, strain 20.5%
Koeck *et al* 2022 [75]	Equine collagen	HCl, acetic acid	Wet-spinning into ammonium hydroxide and acetone	—	25–75 μm	Strength of 241 MPa, strain 17%, toughness 24 MJm^{-3}
Shields *et al* 2004 [77]	Chicken collagen type II	HFIP	Electrospinning	With and without crosslinking	70–496 nm (without crosslinking)	Strength of 3.3 MPa, strain 2.6%
Hepworth *et al* 2002 [69]	Native fibers of tendon	—	—	—	254 μm	Strength of 180 MPa, strain 25.6%
Gosline *et al* 2002 [70]	Native fibers of tendon	—	—	—	—	Strength of 120 MPa, strain 13%

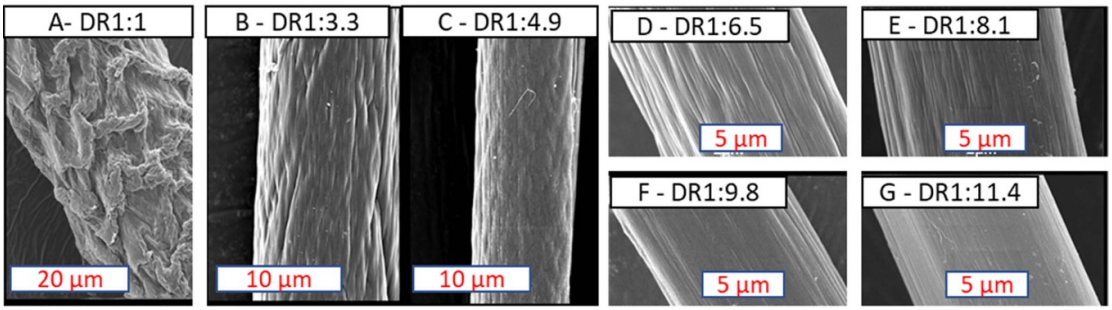

Figure 8. SEM images of fibers with different post-drawing ratios (DR): A to G: DR1:1, DR1:3.3, DR1:4.9, DR1:6.5, DR1:8.1, DR1:9.8, DR1:11.4. Reprinted (adapted) with permission from [74]. Copyright 2016 American Chemical Society.

from collagen dissolved in HCl and wet-spun into phosphate-buffered saline with inline post-stretching to increase fibrillar alignment. The fibers were incubated in the coagulation medium, crosslinked with GA, and dried afterwards. As expected, the fiber diameters decreased with increasing draw ratio down to a diameter of 10 μm (figure 8). Tensile testing revealed that post-drawing to the highest degree did not yield the best mechanical performance. Crosslinked collagen fibers showed a stress at break of 151 MPa and a strain of 20.5% in the hydrated state, which is comparable to native human tendons. The surface of fracture was further analyzed using SEM. Undrawn fibers exhibited a core–shell structure with distinct but weakly oriented fibrils in the core. In contrast, the fibrils in the core of drawn samples appeared more aligned.

In contrast to the aforementioned research, Koeck *et al* used self-assembly during wet-spinning without crosslinking to yield collagen fibers with good mechanical properties [75]. Additionally, these fibers were woven into flat and tubular textiles, which could find application as substrates for muscle tissue regeneration. For the spinning solution, equine collagen was dissolved in acetic acid or HCl at various concentrations. The solutions were extruded into a coagulation bath with a mixture of ammonium hydroxide and acetone. The fibers were dried without further post-treatment. Upon coagulation, collagen fibrils formed through self-assembly. The topography of the assembled fibrils exhibited a periodic, cross-striated D band pattern, which is characteristic of fibril-forming collagens and matches well with native collagen [76]. This pattern has not been shown for artificially spun collagen before. Fibers were achieved with diameters between 25 and 75 μm in the dry state, a breaking strength of 241 MPa, a strain of 17%, and a toughness of 24 MJm^{-3}. The woven fabrics were further subjected to cell studies to assess their suitability for different biomedical applications.

Electrospinning is also used as a collagen processing technique to generate scaffolds for tissue engineering with both materials and dimensions comparable to those of native tissue. Shields *et al* analyzed, among other things, the mechanical properties of electro-spun collagen scaffolds [77]. They used collagen type II from chickens and dissolved it in HFIP. After e-spinning, the scaffolds were cut into bone-like pieces for tensile testing. The non-crosslinked scaffolds contained fibers with diameters ranging from 70 nm to 2.74 μm and an average fiber diameter of 496 nm. Uniaxial tensile testing of scaffolds with an average thickness of 0.20 mm revealed an average ultimate tensile strength of 3.3 MPa with an ultimate strain of 2.6%. The scaffolds were further examined regarding their biocompatibility with adult human articular chondrocytes. Sizeland *et al* investigated whether e-spun collagen displays the native collagen structures of D-spacing and triple helices [67]. They spun solutions of collagen from porcine gelatin and hoki skin in acetic acid. In comparison to native porcine and hoki collagen, electron microscopy revealed that the e-spun fibers did not exhibit the characteristic D band pattern, which is a result of gaps and overlaps in the molecular collagen architecture. This finding was confirmed using small-angle x-ray scattering (SAXS). ATR-FTIR was used to identify the triple helical structure. The data from FTIR analyses did not show evidence of refolding into the native helical buildup occurring during fiber formation.

3. Top-down strategies for the application-driven biomimetic design

In contrast to the previous chapter, the focus here is not on biomimicry of biological materials and processes but on the technical production of functional fibrous materials for application in both biology and technology. The design of these materials is inspired by natural structures, which result in the desired functionality. This functionality is a consequence of the biomimetic design. Therefore, an appropriate choice of both biomimetic and technical polymers and their processing needs to be identified. Three types of applications are presented: textiles, filters, and tissue engineering (figure 9).

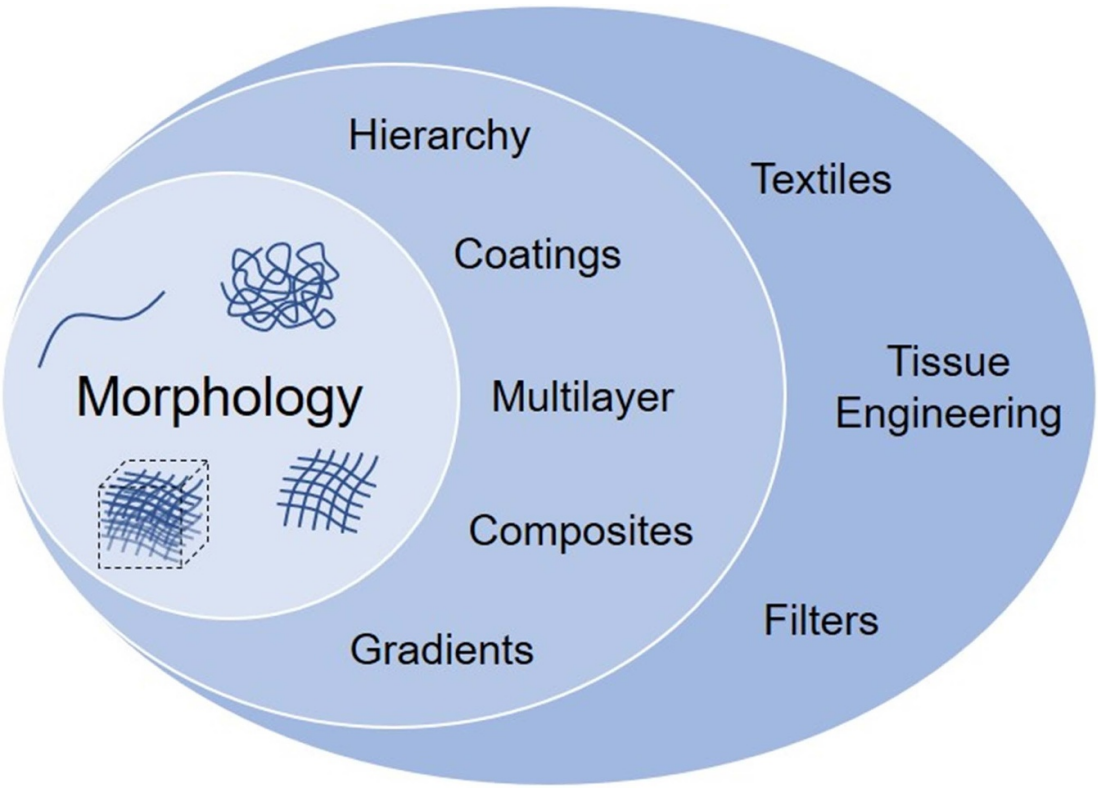

Figure 9. Functionality of bio-inspired materials is achieved by mimicking morphology and structure. The top-down applications of are found in textile-, filter- and tissue engineering.

3.1. Biomimetic design of textiles

Prominent examples of biomimetic textile applications include fibers for thermally insulating fabrics and functional clothing for moisture wicking and heat dissipation. Both applications utilize a hierarchical structure to achieve the desired functionality.

The first two examples in this subchapter address the topic of thermal insulation. Wang *et al* reported an example of biomimicry in the context of thermally insulating fibers [78]. Their inspiration was the hair of polar bears, which exhibits a structure with a hollow core and an outer aligned porous shell. These fibers were fabricated using a wet-spinning foaming process. The polymers used were thermoplastic polyurethane and polyacrylonitrile (PAN), with dimethylformamide (DMF) as the solvent, and water used as a coagulation medium. Diphenylmethane diisocyanate was used as a blowing agent during solidification. After wet-spinning, the fibers were immersed in water for 12 h to remove residual solvent and then dried. The resulting outer diameter was approximately 1.5 mm. Among other properties, the thermal insulation of these polar bear hair-like fibers was examined in comparison to commercial polyester textiles. The fibers exhibited low thermal conductivity, lower than that of cotton or polyester fabrics. The low conductivity is attributed to the higher porosity of the biomimetic fibers. Zhao and Fang were inspired by the hierarchical and fibrous structure of hides and aimed to mimic comparable fibers using wet-spinning [79]. They prepared a mixture of polyvinylidene difluoride (PVDF), polyurethane (PU), and polyvinylpyrrolidone (PVP) in DMF as the fiber material. PVP was used as an additive for pore formation to control the porosity of the fibers. The solution was extruded into a coagulation bath containing 65 vol% ethanol. The fibers were left in the bath for 30 min and then soaked in water for 24 h to remove residual DMF and wash out the water-soluble pore-forming additive. Finally, the fibers were dried and woven. The porous and hierarchical structure of the fibers was examined using scanning electron microscopy (SEM) (figure 10). The hierarchical structure resulted from the phase separation of the polymers. The outer diameter of the fiber was approximately 270 μm, with the PVDF sub-fiber ranging from 2 to 20 μm. The insulation capability of the fibers and woven textiles was analyzed. In comparison to other insulating materials such as PU foams or poly-p-phenylene terephthalamide aerogels, the produced fibers exhibited an excellent combination of mechanical strength and thermal insulation.

Chen *et al* drew inspiration from the branching structure of plants to enhance water absorption and one-way transport of water in knitted fabrics [80]. To achieve this, they developed a circular knitting pattern that created bigger loops at the front side of the fabric and smaller loops at the back, creating a gradient. This knitting pattern can incorporate two different fiber materials, such as polyester and

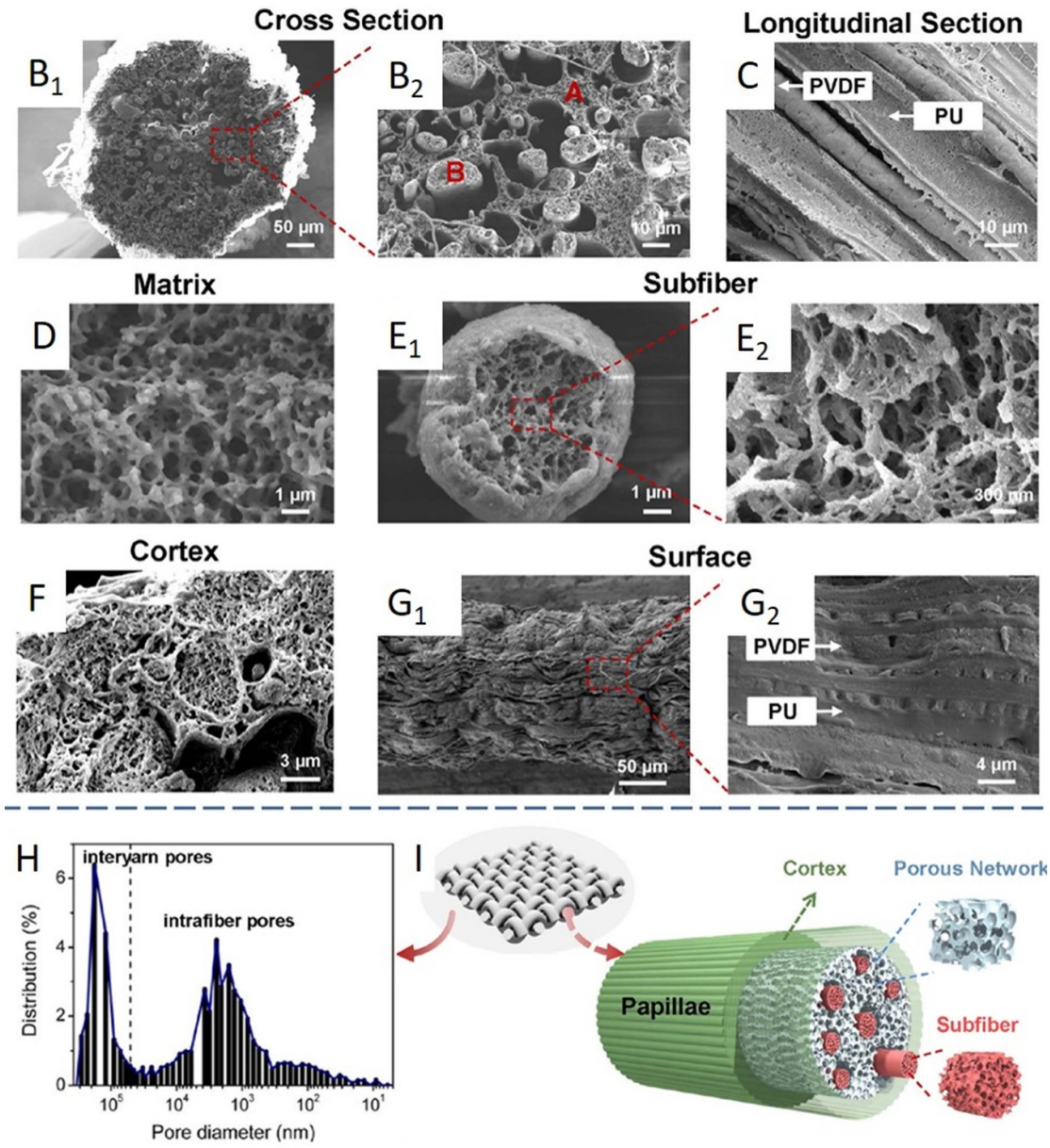

Figure 10. Images of hierarchical porous fibers for thermal insulation: (B–G) SEM images of fiber cross section, longitudinal section, matrix, sub-fiber, cortex and surface (H) pore size distribution of the woven textile (I) schematic drawing of the hierarchical fiber structure and the woven textile. Reprinted (adapted) with permission from [79]. Copyright 2022 American Chemical Society.

cotton. The gradient mimics the water transport in plants. Two liquid water transport tests, the transplanar water transport test and the moisture management test, were conducted. Additionally, air resistance and permeability towards water vapor were measured. Some of their designs successfully led to a significant improvement in the rate of water absorption and water transport compared to two other knitting patterns. Wang *et al* also addressed the issue of moisture-wicking fabrics, but on the microstructural level [81]. They took vascular plants as their natural model. To mimic the structure of plants, they followed a multistep process. Firstly, they prepared a solution of cellulose acetate (CA) in a mixture of acetone and DMSO (3:2 mass ratio). This solution was electrospun onto a PLA nonwoven substrate and dried, resulting in fiber diameters of approximately 670 nm. These membranes were then dip-coated with a solution of micro-fibrillated cellulose and dried. Lastly, fluorinated polyurethane was electro-sprayed on top of the CA membrane to create a multilayer structure. This textile structure was characterized in terms of its drying rate and anti-gravity water transport. The hierarchical structure with branched fibers and a gradient in pore sizes enabled fast water transport and subsequent evaporation. Miao *et al* also aimed to mimic the hierarchical and interconnected network of vascular plants

to achieve a textile with efficient sweat release and heat dissipation [82]. They utilized electrospinning for the fabrication of the textile. PU and boron nitride nanosheets were dissolved/mixed into a tri-solvent system of DMF, ethanol, and acetone and electrospun with a voltage of 40 kV. Multilayer constructs were created through layer-by-layer assembly of single layers with decreasing pore size. Additionally, the membranes were plasma-treated. The gradient in pore size and fiber diameter (900–2500 nm) mimicked the hierarchical structure of plants and enabled antigravity water transport. Evaluation of water transport, evaporation rate, and thermal conductivity identified this construct as a promising approach for drying and cooling textiles.

Lastly, an example of reinforced biomimetic fibers was presented by Ureña-Benavides and Kitchens [83]. They prepared alginate fibers with incorporated cellulose nanocrystals (CNCs) acting as fiber reinforcement using wet-spinning. This reinforcement strategy mimics the structural buildup of plants, where cellulose fibers in the cell walls are surrounded by layers of cellulose microfibers and CNCs that are not oriented along the core fiber axis. In their study, they produced an aqueous spinning solution of sodium alginate and CNCs, which was then extruded into a coagulation bath of calcium chloride, allowing them to spin cellulose fibers with incorporated CNCs. Similar to the natural model, the orientation of the CNCs significantly affected the resulting mechanical properties. Depending on the applied spinning conditions and the fraction of CNCs, they were able to influence this orientation and achieved fibers with a maximum toughness of 390 gpd.

3.2. Filters

Air and water pollution pose risks to both human health and ecosystem preservation. To enhance filter efficiency and selectivity, it is necessary to identify new designs and concepts. Filter efficiency can be evaluated based on pressure drop, energy consumption, and the absorption rate of particles of different sizes. One concept to increase the efficiency of filtration membranes is the application of submicron or nano-fibers [84].

Liu *et al* utilized the electro-netting technique to produce PAN nanofibers that mimic the structure of spider webs [85]. These nonwoven meshes are intended for use as filtration membranes for particulate matter (PM). PAN was dissolved in DMF, and a certain amount of lithium chloride was added. This spinning solution was electrospun onto a PAN nonwoven substrate. The resulting fibers had diameters of around 375 nm for the substrate fibers and 30 nm for the electro-netting fibers. The stacked design resulted in a reduced pore size. These nonwovens mats were characterized in terms of their filtration efficiency and resulting pressure drop. The nano-nets exhibited good particle capture capability through adhesion and interception. Compared to the pure substrate, the nano-nets improved particle capture capability without negatively affecting the pressure drop. The spider web-like filter achieved a $PM_{0.3}$ removal efficiency of 99.996%. Additionally, Liu *et al* reported a combined electrospinning and electro-netting method [86]. In this case, PAN was dissolved in a mixture of dopamine hydrochloride (DA) and DMF. Unlike the first study, no substrate was used. It was a simultaneous process of electrospinning and electro-netting. After spinning, the nonwoven meshes were incubated in Tris HCl buffer solution for 20 h to induce the self-polymerization of DA. The meshes were then washed with water and dried. The process resulted in similar fiber dimensions as described above. These filter membranes maintained their high filtration efficiency even after storage at relative humidity above 90% for ten days. The authors further investigated the performance of liquid separation and dye adsorption, demonstrating that nanofiber-nets (thickness 8.5 μm) exhibited a high rejection efficiency of over 99.9% and simultaneously a very high permeation flux of 453 $Lm^{-2}h^{-1}$, attributed to the highly interconnected open-porous structure.

An impressive example of a biomimetic approach combining top-down with bottom-up techniques, translating a natural principle into a completely different technical context, was presented by Burgard *et al*, who successfully mimicked the mesostructure of penguin downy feathers (figure 11) [87]. The authors employed core–shell electrospinning of polystyrene (PS) (core) fibers seeded with N, N′, N″-tris (1- (methoxymethyl) propyl) benzene-1,3,5-tricarboxamide (BTA) on the shell. Subsequent incubation of these fibers in an BTA solution resulted in self-assembly of off-standing BTA fibrils, with the smallest diameter measuring 140 $\pm$ 60 nm. Air filtration experiments using such mesostructured nonwoven meshes revealed significantly improved filter efficiencies for particles smaller than 1 μm compared to neat PS nonwoven meshes. Remarkably, despite the enhanced filter efficiency, the pressure drop (Δp) across the filter membrane did not increase. This renders bio-inspired meso-structures highly attractive not only for filters but also in the fields of catalysis, energy storage, and energy harvesting.

Another example of biomimetics in filter design is demonstrated by Guan *et al*, who addressed the topic of personal protective equipment [88]. They utilized a biomimetic hierarchical structure design using cellulose-based fibers to create filter membranes. To fabricate these multiscale membranes, a slurry of cellulose nano- and microfibers was mixed with silver nanowires, which possess antibacterial properties. The slurry was then transferred into a bath, and a substrate was dip-coated in the medium. After drying, the composite membrane was peeled off the substrate. These membranes exhibited permeability for

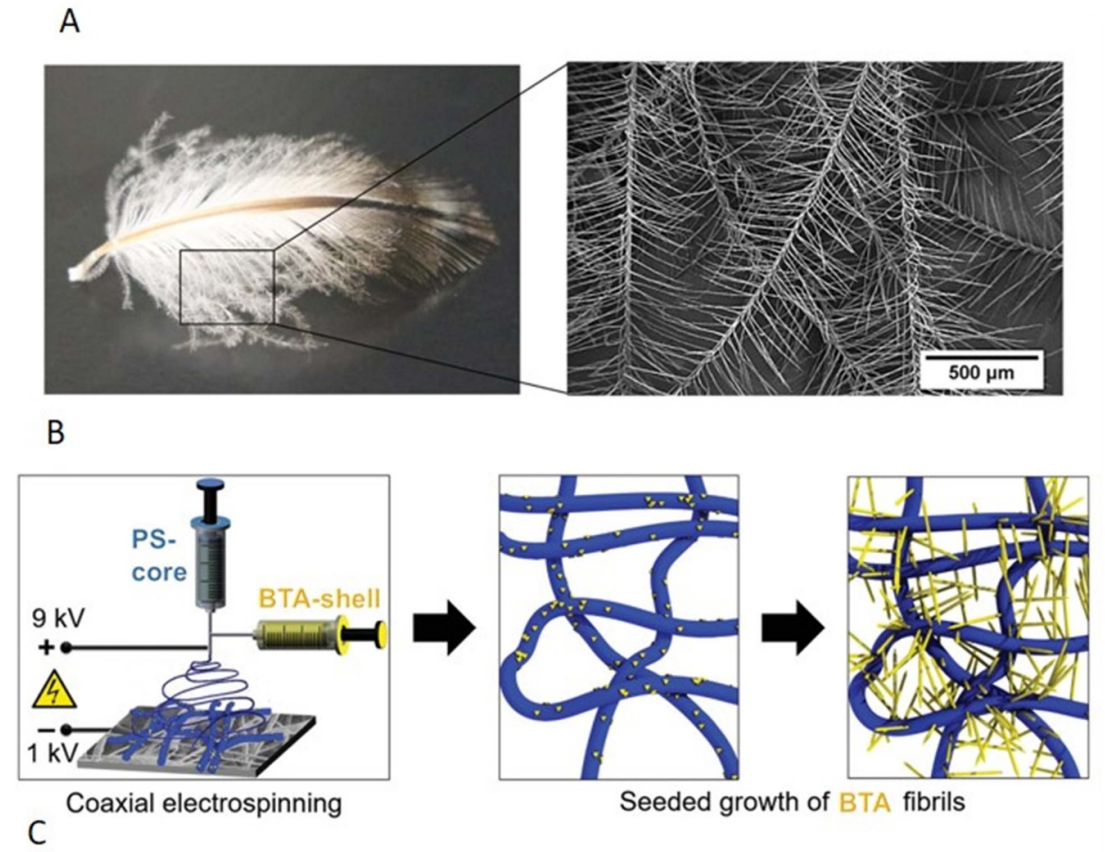

Figure 11. (A) Image of a feather of a Humboldt penguin (left) and a respective SEM image of the lower barbs (right). (B) Schematic illustration of the membrane preparation through electrospinning and fibril growth on the fiber surface. (C) Microscopy images of BTA fibrils on glass slides: non-seeded fibrils, non-seeded fibrils with e-spun polystyrene fibers and mesostructured membrane with seeded fibrils on the fiber surface (from left to right). [87] John Wiley & Sons. © 2019 WILEY-VCH Verlag GmbH & Co. KGaA, Weinheim.

both air and moisture and achieved a high $PM_{2.5}$ filtration efficiency of approximately 92%. The reduced pore size resulting from the inherent multiscale fibers contributed to this high efficiency. The incorporation of silver nanowires provided additional antibacterial properties. This processing technique offers the potential for automation, enabling large-scale production of protective equipment.

Li *et al* employed micro-stereolithography to fabricate fish gill-shaped structures [89]. These biomimetic structures were developed as a means to produce chemical-free microfluidic filtration membranes with anti-fouling properties. The fabrication process involved building up the three-dimensional structure layer by layer through photo-curing. Firstly, a filtration membrane was immersed in the printing ink and left still for one hour. Then, the ink-soaked membrane was placed on the printing stage, and the 3D fish gill structure was printed onto its surface using micro-stereolithography. The filtration and anti-clogging performance were evaluated using a surfactant-stabilized emulsion and plastic microparticles. The gill-shaped filters demonstrated anti-fouling properties through the ricochet behavior of droplets and particles, allowing them to flow along the filter in the mainstream. Ling *et al* addressed the issue of water purification and demonstrated the generation of ordered multilayer membranes using

silk nanofibrils and hydroxyapatite [90]. These biogenic material-based membranes aimed to increase water throughput while maintaining high filtration efficiency. The fabrication process was inspired by the biomimetic processes of silk self-assembly and biomineralization of hydroxyapatite. Firstly, an aqueous solution of silk with a concentration below 0.3 wt% was prepared. This solution was incubated at 60 °C for a week to induce nanofibril growth. Then, $CaCl_2$ and Na_2HPO_4 were added, and the solution was incubated for another week at 37 °C to grow hydroxyapatite nanocrystals. Finally, the solution was vacuum-filtrated, resulting in a biomaterial membrane on top of a polycarbonate filtration membrane. This method yielded alternating ordered layers of approximately 200 nm of fibrils and mineral. It was demonstrated that these composite filters could be used for water purification. Variations in the polymer used for the nanofibrils could further enhance the filter efficiency for pollutants.

Homaeigohar *et al* drew inspiration from carnivorous plants [91]. The leaves of these plants are coated with a sticky adhesive to attract and capture prey. Similarly, the researchers immobilized BSA proteins on the surface of electrospun Poly(acrylonitrile-co-glycidyl methacrylate) nanofibers to enhance the filtering selectivity for water filtration. The nonwoven mesh was electrospun from a 20 wt% solution in DMF, resulting in fiber diameters of approximately 100–125 nm. The dried nonwoven meshes were then incubated in an BSA/PBS buffer for 24 h. The filtration performance was analyzed in terms of the capability to remove proteins and nanoparticles. Aqueous solutions of BSA and aqueous suspensions containing 40 nm gold nanoparticles were utilized. In aqueous media with a pH ranging from 4 to 7, the nanofibers experienced swelling, resulting in a reduction of the average pore size of the membrane. This swelling phenomenon created greater steric hindrance and facilitated the interaction between the filtrates and the surface functionalization. SEM was employed by the authors to confirm the adsorption of gold nanoparticles onto the functionalized surface. Moreover, the functionalized membrane demonstrated a significantly enhanced filter efficiency for BSA when compared to a non-functionalized membrane.

3.3. Tissue engineering

A significant amount of research is focused on tissue engineering, which aims to artificially fabricate biological tissue for use in tissue regeneration or replacement. The incorporation of biomimetic elements, such as biological structures, materials, and physicochemical properties, is believed to enhance the biocompatibility of these artificial constructs. This chapter is divided into two parts: the first part explores the biomimicry of fibers used in artificial blood vessels, while the second part addresses scaffold design for tissue engineering. Blood vessels are present throughout the human body and play a crucial role in the circulatory system. Numerous studies are dedicated to mimicking the structure of natural vessels to achieve biocompatible and functional implants.

Jia *et al* aimed to mimic helical blood vessels using microfluidics for biomimetic organ-on-a-chip applications [92] They utilized a microfluidic chip to spin hollow, helical hydrogel microfibers. A two-flow setup was employed, with $CaCl_2$ solution as the inner flow and alginate solution as the outer flow. Contact between the two solutions resulted in immediate crosslinking. By adjusting the ratio of inner to outer flow rate, the geometry, pitch, amplitude, and diameter of the helical structures could be controlled. The use of a blend of alginate and collagen as the outer medium improved biocompatibility and enabled the growth of HUVEC cells inside the hollow fibers. In 2021, Xie *et al* developed a protocol for the continuous generation of perfusable hydrogel microtubes based on the same process described above [93]. These tubes, composed of alginate, were crosslinked by both a sheath flow and a collecting bath of $CaCl_2$. The geometry and morphology of these tubes could be precisely manipulated through fluid dynamics, and cells could be directly loaded into the fibers. This approach allows for the mimicking of specific vessel shapes in microtissues. For instance, Xie *et al* produced hollow alginate fibers with glomerular-like structures to mimic blood vessels [94]. They used a setup with $CaCl_2$ as the core flow and sodium alginate mixed with calcium carbonate as the sheath flow. A bath of $CaCl_2$ was utilized to complete the crosslinking process. The uncrosslinked alginate solution dropping down from the outlet stayed on the fiber and solidified in the bath, resulting in a continuous fiber with incorporated $CaCl_2$ and glomerular-like structures—a promising result for kidney-on-a-chip devices. The tubes were then immersed in a hydrogen chloride solution, which triggered a chemical reaction between $CaCl_2$ and protons, releasing trapped CO_2 bubbles and inflating the tubes. Endothelial cells were subsequently seeded into the perfusable fibers to generate vascular constructs. Another type of hollow fibers for tissue construction was generated by Zuo *et al*, combining photo-cross-linkable methacrylated gelatin (GelMA) and alginate [95]. Their microfluidic setup comprised three inlets, enabling coaxial laminar flow. In the first inlet, hyaluronic acid was injected as the core flow, while in the second and third, a solution of alginate, GelMA, and a photoinitiator was injected. The filament was spun into a bath of $CaCl_2$, followed by exposure to UV light to crosslink the GelMA. The laminar flow conditions facilitated the fabrication of a double-layer hollow fiber. By adjusting the outlet diameters and tuning the flow rates of the three solutions, the authors were able to control the thickness of the different layers. For instance, the thickness of the outer layer could be varied between 50 and 180 μm.

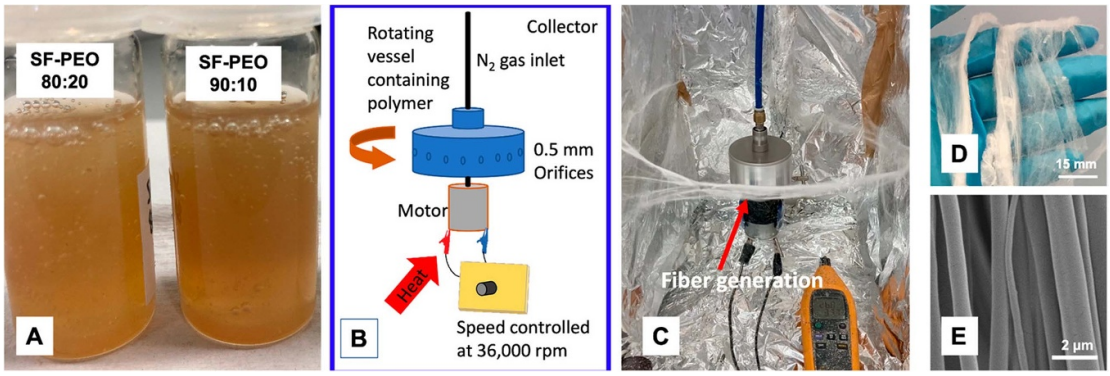

Figure 12. Preparation of tissue constructs via pressurized gyration: (A) aqueous blends of silk fibroin and PEO; (B) schematic of pressurized gyration setup containing a rotating cylinder with the spinning solution, a motor and a gas inlet; (C) resulting fibers after 5 s of spinning (D) macroscopic image of fibers (E) SEM image of these fibers. Reproduced from [100]. CC BY 4.0.

The authors further demonstrated the potential of these fibers for cell encapsulation within the different layers, using endothelial and osteoblast-like cells. Endothelial cells were introduced in the middle layer, while osteoblast-like cells were placed in the outer layer to mimic bone tissue.

Another example of the production of a required biological architecture has been presented by Zhou *et al.* They utilized coaxial electrospinning to create hollow poly(ε-caprolactone) (PCL) b-polyethylene glycol (PCL-)b-PEG and PLGA microfibers as reference objects for validating diffusion magnetic resonance brain imaging [96]. This imaging technique is based on the anisotropic diffusion of water in axonal fibers, which typically exhibit diameters ranging from 0.16 to 9 μm [97]. The spun fibers aim to mimic the axonal fibers in the brain and, consequently, need to exhibit this anisotropic diffusion behavior. Zhou *et al* successfully fabricated fibers with diameters in the micron range by employing a coaxial spinneret setup with two concentric needles. PCL-b-PEG and PLGA were used as the shell materials, while PEO was utilized for the core. Using these electrospun fibers, they effectively created reference objects for magnetic resonance imaging (MRI). Multiple fiber strips were stacked into a tube filled with deionized water and incubated for one week. MRI confirmed the desired anisotropic diffusion behavior of water.

Electrospinning is a versatile technique for mimicking the natural ECM environment of various tissues and organs. It allows for the fabrication of artificial ECM scaffolds using synthetic polymers, biopolymers, and blends. These scaffolds are specifically designed to interact with cells, promote proliferation and growth, and thereby support the formation of functional tissue. Biomimicry can be applied to address different aspects of the ECM. The dimensions of fiber diameter and pore size in the nonwoven mat play a crucial role in designing effective scaffolds that match the desired tissue for successful tissue regeneration or replacement.

Lowery *et al* demonstrated that the pore size of electrospun nonwoven mats affects the migration of human dermal fibroblasts into the constructs and the tendency to produce ECM between the fibers [98]. By blending PCL with PEO and post-treating in water, they produced scaffolds with similar fiber diameters but different void sizes ranging from approximately 3–24 μm. The authors noted that there is an optimal pore diameter range (~6–20 μm) in the order of the average cell diameter (~15 μm), which enables cells to grow into the scaffolds and proliferate in a three-dimensional manner. If the void size is too small, cells cannot migrate into the scaffold; if it is too large, ECM generation is reduced, and cells prefer growing alongside fibers rather than branching out three-dimensionally. In contrast, Sisson *et al* examined the impact of small (110 nm) and large (600 nm) electrospun gelatin fiber diameters on the behavior of human osteoblast-like MG63 cells [99]. The nonwoven mat with the larger fiber diameter exhibited an average pore size of 1.00 ± 0.61 μm^2, while the one with the smaller fiber diameter had an average pore size of 10.7 ± 5.7 μm^2. The authors found that osteoblasts behave differently in terms of penetration depth, growth, and differentiation depending on the fiber morphology. A larger fiber diameter, leading to larger void sizes, allowed MG63 cells to migrate deeper into the construct, promoting improved cell growth. On the other hand, a smaller fiber diameter promoted differentiation. Both scaffold properties, fiber diameter, and pore size, can be adjusted through process parameters and the choice of materials. These properties have a significant impact on cell behavior and must be carefully tailored according to the desired application. Additional factors to improve cell viability are fiber alignment and the choice of solvent. In a non-cytotoxic and green setup Heseltine *et al* used a pressurized gyration process to spin fibers from aqueous blends of silk fibroin and PEO (figure 12) [100]. This process yields aligned fiber bundles. Depending on

the blend ratio and the processing parameters, fiber diameters between 0.71 and 2.10 μm were achieved. These fibers were used in cell culture experiments with both human osteosarcoma and human fetal osteoblast cells. In comparison with fibers spun from toxic HFIP, the fibers from aqueous solution revealed significantly improved cell viability and proliferation for both cell lines. This finding could be due to residual HFIP inside the fibers. Therefore, this research underlines the importance of using non-toxic processing routes to fabricate successful tissue constructs.

In addition to the structure, the fiber material is another aspect that can be mimicked. Collagen, the most abundant structural protein in the ECM, is widely recognized as one of the most favored biomaterials [101]. However, spinning solutions with a high concentration of collagen are typically achieved using HFIP or strong acids. The dissolution of collagen in these solvents results in the irreversible destabilization of the native triple helical configuration, rendering e-spun collagen soluble in aqueous physiological media [102]. Wang *et al* proposed an approach to overcome this issue by blending collagen with poly(L-lactic acid) (PLLA) [103]. By dissolving collagen and PLLA in TFA, the authors were able to spin fibers with an average diameter of around 350 nm. These fibers exhibited a sheath-core structure, with PLLA forming the sheath due to phase separation during the spinning process. Pant *et al* also utilized the phenomenon of phase separation to produce core–shell structured fibers from a blend solution of nylon-6 and lactic acid (LA) [104]. In this case, nylon-6 was used as the core material, while LA served as the coating. The authors further modified the surface properties through calcium base treatment, resulting in the conversion of surface LA to calcium lactate. This conversion increased biocompatibility, as investigated using mouse osteoblasts, and highlighted the potential of this composite nonwoven mat for bone tissue engineering. Overall, it is evident that further development of tailored processing strategies is necessary to meet the morphological and material requirements for different types of cells and scaffolds.

Park *et al* produced biodegradable and nanostructured scaffolds by electrospinning a blend of poly(glycolic acid) (PGA) and chitin in HFIP for use as an artificial ECM in tissue engineering [105]. Both PGA and chitin are biocompatible and biodegradable. The resulting average fiber diameter was approximately 130–150 nm. During solidification, phase separation occurred due to the immiscibility of PGA and chitin in the as-spun structure. The degradation and compatibility of these fibers with human epidermal fibroblasts were analyzed. Degradation tests were conducted in PBS (pH 7.2) at 37 °C, revealing that the rate and amount of degradation decreased with increasing chitin ratio in the blend compared to pure PGA. Blends with chitin exhibited prolonged structural integrity. Nonwoven mats coated with BSA demonstrated promising results for cell attachment and spreading. Zhixiao *et al* employed electrospinning to fabricate tissue scaffolds from PCL and CA [106]. These scaffolds were designed for wound healing and skin renewal applications and aimed to inhibit the differentiation of epidermal stem cells (EpSCs). The scaffold morphology consisted of microfibers with an average diameter of 648 nm entangled with nanofibers measuring 82 nm. To assess the suitability of these scaffolds for EpSC adhesion, stem cells were seeded on the construct, and SEM analysis was conducted. The cells were observed to be tightly attached to the fibers and embedded within the micro- and nanostructure of the scaffold. Scaffolds with these cells were shown to improve wound healing through activation of the Notch signaling pathway.

In contrast to the aforementioned research, Narayanan *et al* employed electrospinning to generate aligned nonwoven meshes instead of randomly deposited ones [107]. These aligned scaffolds were designed to mimic the microenvironment of muscle fibers for skeletal muscle regeneration, necessitating both structural and muscle cell compatibility. The authors used solutions of 20%–40% PLGA in a 3:1 mixture of THF and DMF. By electrospinning on a rotating drum, they successfully created aligned scaffolds with fiber diameters ranging between 335 nm and 3013 nm. C2C12 murine myoblast cells were cultured on these scaffolds, and their adhesion and proliferation were characterized. Matrixes with larger diameters, ranging from 1500 nm to 3013 nm, exhibited improved proliferation and differentiation of the myoblasts. An *in vivo* evaluation was conducted using a mouse model, comparing the scaffold with myoblasts to the transplantation of myoblasts alone. The comparison showed a significantly greater number of dystrophin-positive myofibers at the transplantation site, highlighting the critical role of topography in successful cell conditioning for muscle regeneration. Another study focusing on tissue microenvironment was published by Nelson *et al* in 2014 [108]. The aim of their study was to develop *in vitro* scaffolds for evaluating the potential of novel anti-metastatic breast cancer drugs. Since late-stage breast tumor ECM exhibits aligned structures, they mimicked this ECM using aligned electrospinning. The scaffolds were spun from a 5% (w/w) solution of PCL in HFIP and had an average diameter of 795 nm. Cells were seeded onto these aligned scaffolds and onto randomly deposited nonwoven mats for comparison. In contrast to the latter, the majority of cells on the aligned construct exhibited an elongated shape along the fiber axis. Additionally, the aligned PCL nanofibers promoted increased migration distance compared to the random nonwoven mesh. This finding aligns with observations from tissue biopsies, which

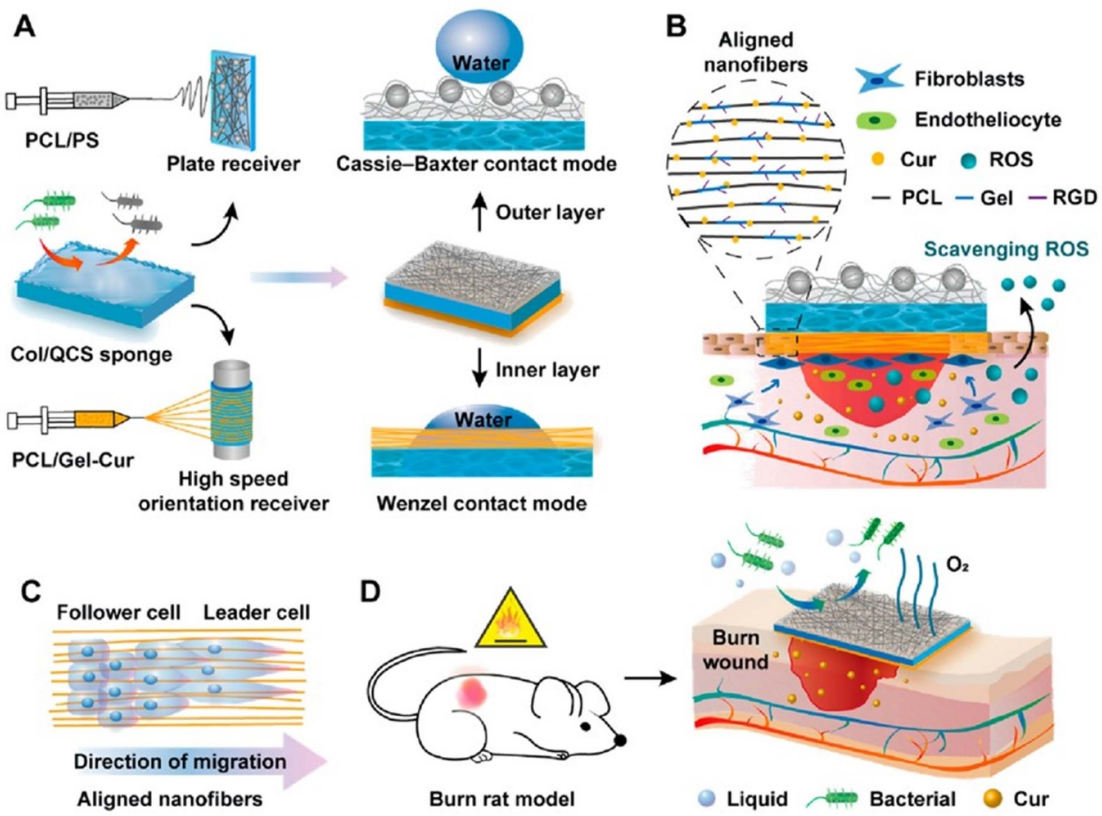

Figure 13. Schematic of preparation of a three layer composite wound dressing: (A) multilayer preparation: E-spun PCL with immobilized PS microspheres (top), collagen/chitosan sponge (middle), aligned e-spun PCL/gelatin scaffold (bottom); (B) sponge and outer layer inhibit bacterial infections, curcumin (Cur) and gelatin in the aligned scaffold promote wound healing; (C) aligned scaffold regulates cell proliferation and growth; (D) in vivo tests of wound dressing for burn wounds. Reprinted (adapted) with permission from [109]. Copyright 2022 American Chemical Society.

have demonstrated that the radial rearrangement of fibers in tumor tissue facilitates metastatic migration.

Strategies also exist for mimicking hierarchical tissue structures using multilayer constructs. The concept is to enhance effectiveness and combine the functionality of different layers into a precisely designed construct. He *et al* utilized aligned electrospun nanofibers to mimic natural tissue for wound dressings [109]. They integrated aligned scaffolds into a composite three-layer structure (figure 13). The middle layer consisted of a collagen and chitosan sponge, the inner layer comprised an aligned PCL/gelatin scaffold, and the outer layer featured a hierarchical micro- and nanostructure of PCL and PS-microspheres. The aligned scaffold was electrospun from a blend solution of 16% PCL in a 7:3 mixture of acetic and FA, with later addition of 4% gelatin. The diameters of the aligned fibers ranged from 163 to 204 nm. The aligned fiber structure significantly influenced cell arrangement and growth direction. The outer layer was inspired by the superhydrophobic surface of lotus leaves, which reduces contact area and increases hydrophobicity. This layer was electrospun from a blend solution of 20% PCL and PS microspheres in the same acetic and FA mixture as before, resulting in a composite of randomly arranged fibers and beads. The top layer aimed to inhibit bacterial adhesion and wound contamination by mimicking the lotus leaf's hydrophobic properties. The function of the middle layer was to prevent exudate accumulation and dehydration. The constructs were further tested for their wound healing capacity using *in vivo* burn tests with rats.

Hu *et al* aimed to fabricate multilayer scaffolds using coaxial electrospinning for vascular tissue engineering, generating triple-layered scaffolds [110]. The core solution consisted of 7 wt% PLGA in HFIP and DCM at a ratio of 1:1, while the shell solution comprised 7 wt% gelatin and collagen (2:1) dissolved in HFIP. Both solutions contained 1 wt% of Tween 80, a non-ionic surfactant. The nonwoven meshes were spun onto a rotating, spiraled copper wire. Between a bottom and top layer of coaxial nanofibers, a layer of pure PLGA nanofibers was spun to create a hollow three-layered scaffold. Subsequently, the constructs were crosslinked using a solution of N-(3-dimethylaminopropyl)-N′-ethylcarbodiimide/N-hydroxysuccinimide (EDC/NHS) or GA vapor. When compared to fibers spun without Tween 80, the nonwoven meshes with Tween 80 showed no beads, a smooth surface, a more uniform coaxial structure, and improved spinning process stability. The

Table 4. Overview of published biomimetic scaffolds. Abbreviations stand for poly(ε-caprolactone) (PCL), polyethylene oxide (PEO), poly-L-lactide acid (PLLA), lactic acid (LA), poly(glycolic acid) (PGA), cellulose acetate (CA), poly(lactic-co-glycolic acid) (PLGA), Tussah silk fibroin (TSF), N-(3-dimethylaminopropyl)-N′-ethylcarbodiimide/N-hydroxysuccinimide (EDC/NHS), polypyrrole nanoparticles (PPy NPs).

Author, Year	Polymer	Structure	Diameter	Cells/models	Observation
Lowery *et al* 2010 [98]	PCL-PEO blend	Random nonwoven mat	1–10 μm	Fibroblasts	Human dermal fibroblast (HDF) migrated into the scaffold, optimal pore size is in the range of average cell diameter.
Sisson *et al* 2010 [99]	Gelatin	Random nonwoven mat	110 ± 40 and 600 ± 110 nm	Osteoblasts	Larger diameters and pores enhanced MG-63 osteoblast like cell migration and growth, smaller diameters and pores induced cell differentiation.
Heseltine *et al* 2022 [100]	Silk fibroin—PEO blend	Aligned nonwoven mat	0.71 ± 0.17–2.10 ± 0.78 μm	Human osteosarcoma and human fetal osteoblast cells	Use of an aqueous spinning solution showed improved cell viability in comparison to nonwoven mats spun out of HFIP
Wang *et al* 2012 [103]	Collagen/PLLA blend	Random nonwoven mat, sheath-core structure	350 nm	—	Phase separation during spinning results in an extended interphase, core–shell structure with PLLA forming the shell and collagen in the core.
Pant *et al* 2013 [104]	Nylon-6 /LA blend	Random nonwoven mat, sheath-core structure	10–250 nm	Osteoblasts	Post-conversion of nylon-6/LA core–shell fiber mats into nylon-6/calcium lactate (CL) nonwoven mats resulted in significantly stimulated bone formation as shown with MC3T3-E1 mouse osteoblasts.
Park *et al* 2006 [105]	PGA-chitin blend	Random nonwoven mat	130–150 nm	Fibroblasts	*In vitro* degradation studies showed that PGA in PGA/chitin blend nanofibers degraded faster than pure PGA nanofibers. Primary normal human fibroblasts (NHEF) displayed good attachment and spreading on PGA/chitin fiber mats.
Zhixiao *et al* 2021 [106]	PCL-CA blend	Random nonwoven mat	648 ± 165 and 82 ± 33 nm	Epidermal stem cells	PCL/CA electrospun micro/nanofiber scaffold could maintain the stemness of epidermal stem cells (EpSCs) by inhibiting the Notch signaling pathway.
Narayanan *et al* 2020 [107]	PLGA	Aligned nonwoven mat	Between 335 ± 154 and 3013 ± 531 nm	Myoblasts	Larger fiber diameters led to improved proliferation and differentiation of C2C12 myoblasts.

(Continued.)

Table 4. (Continued.)

Author, Year	Polymer	Structure	Diameter	Cells/models	Observation
Nelson *et al* 2014 [108]	PCL	Aligned nonwoven mat	795 ± 125 nm	Human normal mammary epithelial- and breast cancer cells	MCF-10A human normal mammary epithelial cells, MCF-7 and MDA-MB-231 human breast cancer cells showed significantly increased alignment and migration on oriented fiber mats rendering such constructs attractive for drug evaluation.
He *et al* 2022 [109]	PCL—gelatin, chitosan—collagen, PCL scaffold	Three-layer buildup, inside to outside: aligned scaffold, sponge, scaffold with PS microspheres	163–204 nm	Rat model	A multi-layer skin graft with antimicrobial, cell-guiding, exudate absorbing function was shown to promote epithelial wound healing, regulate angiogenesis, and improve inflammation in *in-vivo* burn tests with rats.
Hu *et al* 2020 [110]	PLGA and collagen/gelatin	Triple-layered scaffold	465 ± 23.04 nm	Endothelial cells	Human umbilical vein endothelial cells (HUVECs) displayed better viability and proliferation on EDC/NHS cross-linked scaffolds as compared to glutaraldehyde-treated ones. Hemolysis experiments showed improved blood compatibility for EDC/NHS cross-linked fiber mats.
Shao *et al* 2016 [111]	PLA-TSF blend	Weaving e-spun nanofiber yarns	Fiber diameter 500 nm, yarn diameter of 85 μm	Mesenchymal stem cells	Woven scaffolds promoted adhesion and proliferation of mouse mesenchymal stem cells (MSCs), and induced biomineralization via alkaline phosphatase and mineral deposition. The scaffolds significantly enhanced bone formation in damaged femoral condyle in rabbits.
Tang *et al* 2020 [112]	PCL, co-sprayed collagen and conductive PPy NPs	Aligned nonwoven mat with conductive layer		Neuronal cells	The aligned scaffold promoted PC12 neuronal cell orientation and neurite/axon extension along the fibers. Conductive fibers could be successfully applied for electrical cell stimulation.

average fiber diameter was 465 nm. Crosslinking had no significant impact on porosity, but in terms of biomechanical performance, EDC/NHS-crosslinked scaffolds outperformed those crosslinked with GA vapor. Furthermore, a hemolysis experiment demonstrated that the EDC/NHS-crosslinked scaffolds exhibited better blood compatibility compared to GA-crosslinked scaffolds. Cell viability tests confirmed the potential of the EDC/NHS multilayer scaffolds for bioinspired vascular applications. Shao *et al* designed another multilayer scaffold for bone tissue engineering [111]. The scaffold was created by weaving nanofiber yarns electrospun from polylactic acid (PLA) and Tussah silk fibroin (TSF). This design aimed to mimic the hierarchical structure of bone ECM, which is crucial for scaffold functionality. The yarns were fabricated by electrospinning 8 wt% solutions of TSF and PLA from two dope supplies into a rotating funnel collector. The nonwoven mesh was then drawn as a bundle from the rotating collector using a winding unit. This yarn was woven into a three-layered fabric. The addition of 10 wt% silk fibroin in the solution resulted in a fiber diameter of 500 nm and a yarn diameter of 85 μm. Generally, the amount of added fibroin significantly impacted the fiber morphology, likely due to changes in solution viscosity and conductivity. *In vitro* experiments demonstrated that the woven fabric supported the adhesion and proliferation of mesenchymal stem cells and mineralization. Moreover, *in vivo* studies showed that the biomimetic construct improved bone formation in damaged femurs.

When it comes to nerve tissue scaffolds, electrical conductivity within the construct plays a crucial role. Tang *et al* addressed this aspect by combining electrospinning and electrospraying to create a composite scaffold that showed promising results for nerve tissue engineering [112]. They sprayed collagen and conductive polypyrrole nanoparticles onto the surface of aligned microfibers of PCL. Aligned scaffolds were achieved using a rotating drum as a collector in the electrospinning setup. After seeding PC12 cells onto the scaffold, two effects were observed. Firstly, the aligned fibers promoted the orientation of PC12 cells along the fibers and elongated neurites. Secondly, the combination of the conductive microenvironment of the scaffold and external electrical stimulation of the cells led to increased neurite outgrowth and expression levels.

4. Conclusion and outlook

The global market for polymer fibers is characterized by a significant volume, primarily consisting of synthetic and cellulose-based fibers. Over the past two decades, the production of these fibers has exceeded 80 million metric tons worldwide, with synthetic fibers accounting for more than 90% of this total [113]. These statistics highlight a dramatic increase in the consumption of fossil resources and energy, which are essential for the production, recycling, and melt-processing of polymers. In contrast, nature exemplifies material and energy efficiency as crucial factors for survival. Fiber spinning and production in nature occur at moderate temperatures, without the need for harsh chemical conditions, resulting in high-performance materials that meet requirements with minimal resource usage. Considering the global climate situation and the urgent need to change our resource utilization practices, it is imperative to carefully reevaluate all options in every technical field and explore alternatives, even if they may not initially seem economically attractive. One promising avenue within the context of polymer fibers is the development of biomimetic fibers.

In this review, we have made efforts to categorize the extensive field of biomimetic polymer fibers into two sections. The first category examines two biological fibers, silk and collagen, and their biomimicry through technological approaches, emphasizing the mechanical performance of the resulting fibers. Several studies have demonstrated that a combination of careful mimicry of silk materials, spinning conditions, and post-treatments is key to achieving materials with comparable mechanical properties to those found in nature. Notably, the concentration of the spinning solution has a significant influence on fiber mechanics, and it is possible to achieve mechanical properties that match or even surpass those of synthetic fibers. Microfluidics plays a pivotal role in investigating the impact and necessity of natural spinning conditions on fibers. Once the key parameters are identified, spinning techniques such as wet-spinning can be adjusted to enable the scalable production of silk materials. Collagen, an important material for biomedical applications, has also been successfully processed using multiple spinning techniques. While the achieved mechanical properties are comparable to those of native collagen, these fibers often lack the native protein structure due to the processing conditions. In the medical field, it is important to substitute toxic crosslinkers with non-toxic alternatives or adopt a closer approach to the natural model by working without artificial post-treatment and utilizing natural self-assembly. The second category focuses on the design of functional fibrous materials for both biological and technical applications. The application of biomimetics in these fields enables advancements in various technical applications, such as air and water filtration or thermally insulating materials. Furthermore, biomimetics enhances the functionality of materials in biomedical applications, including tissue engineering and *in vitro* research. Within these disciplines, biological concepts offer strategies for developing more efficient and environmentally friendly materials. Another area of research focuses on mimicking natural structures, such as the ECM. Understanding

how the geometric properties of a scaffold influence cell behavior and well-being is crucial for designing materials suitable for *in vivo* applications.

The production of biomimetic fibers often does not appear economically attractive or compatible with industrial scale-up. Nonetheless, it is crucial to start identifying techniques for biomimetic fiber processing to explore the multitude of opportunities nature provides. Strategies should be pinpointed to tackle significant areas of sustainability of polymer fiber production. Sustainability encompasses key facets such as the choice of polymer and its production, solvent selection, and processing temperature. Biopolymers, from the beginning, provide the benefit of being processed from solutions at moderate temperatures, obviating the need for expensive heating. In solution spinning, it is crucial to identify suitable solvents, which differ depending on the specific biopolymer. It is noteworthy that much of the current research depends on hazardous chemicals. However, these chemicals are not inherent to the natural spinning processes of biopolymers. Therefore, they should serve as a temporary workaround. Processing from aqueous or recoverable solvents will be a prerequisite for scale-up, aiming to prevent toxic waste production. Scaling up of fiber processing for industrial applications needs refinements in several spinning methods, such as traditional electro-spinning, to shift from lab-scale to high-yield processes. In the domain of nanoscale fibers, essential for applications like tissue engineering or filtering, promising techniques include pressurized gyration and centrifugal electrospinning [114, 115]. In the future, it will be essential to evolve different techniques capable of creating fibers with varying dimensions (e.g. micro, nano) or morphologies (e.g. monofiber, aligned nonwoven meshes, random nonwoven meshes).

The authors of this review are convinced, that biomimetics and bio-inspiration provide strategies for a variety of problems in both technical and biological applications. Biomimetics might also be one way to identify new groundbreaking materials, processes and structures as alternatives for the synthetic fiber industry.

Data availability statement

The data cannot be made publicly available upon publication because they are owned by a third party and the terms of use prevent public distribution. The data that support the findings of this study are available upon reasonable request from the authors.

Acknowledgments

This work was supported by the Federal Ministry for Economic Affairs and Climate Action (BMWK: *Bundesministerium für Wirtschaft und Klimaschutz*) Project Number KK5086506SA1.

ORCID iDs

Gregor Lang https://orcid.org/0000-0001-9819-8630
Thomas Scheibel https://orcid.org/0000-0002-0457-2423

References

[1] Vincent J F V, Bogatyreva O A, Bogatyrev N R, Bowyer A and Pahl A-K 2006 Biomimetics: its practice and theory *J. R. Soc. Interface* **3** 471–82
[2] Paris O, Burgert I and Fratzl P 2010 Biomimetics and biotemplating of natural materials *MRS Bull.* **35** 219–25
[3] Bhushan B 2009 Biomimetics: lessons from nature—an overview *Phil. Trans. R. Soc.* A **367** 1445–86
[4] Gough C R, Rivera-Galletti A, Cowan D A, Salas-de la Cruz D and Hu X 2020 Protein and polysaccharide-based fiber materials generated from ionic liquids: a review *Molecules* **25** 3362
[5] Sonnleitner D, Sommer C, Scheibel T and Lang G 2021 Approaches to inhibit biofilm formation applying natural and artificial silk-based materials *Mater. Sci. Eng.* C **131** 112458
[6] Puppi D and Chiellini F 2017 Wet-spinning of biomedical polymers: from single-fibre production to additive manufacturing of three-dimensional scaffolds *Polym. Int.* **66** 1690–6
[7] Fischer K *et al* 1985 Rheology of viscose .3. On the rheology of the wet spinning process in the production of Viscose fibers *Acta Polym.* **36** 95–99
[8] Mirabedini A, Foroughi J and Wallace G G 2016 Developments in conducting polymer fibres: from established spinning methods toward advanced applications *RSC Adv.* **6** 44687–716
[9] Paul D R 1968 Diffusion during the coagulation step of wet-spinning *J. Appl. Polym. Sci.* **12** 383–402
[10] Silva R D, Vongsanga K, Wang X and Byrne N 2016 Understanding key wet spinning parameters in an ionic liquid spun regenerated cellulosic fibre *Cellulose* **23** 2741–51
[11] Beebe D J, Mensing G A and Walker G M 2002 Physics and applications of microfluidics in biology *Annu. Rev. Biomed. Eng.* **4** 261–86
[12] Du X-Y, Li Q, Wu G and Chen S 2019 Multifunctional micro/nanoscale fibers based on microfluidic spinning technology *Adv. Mater.* **31** 1903733
[13] Jun Y, Kang E, Chae S and Lee S-H 2014 Microfluidic spinning of micro- and nano-scale fibers for tissue engineering *Lab Chip* **14** 2145–60
[14] Temesgen S, Rennert M, Tesfaye T and Nase M 2021 Review on spinning of biopolymer fibers from starch *Polymers* **13** 1121
[15] Dong H, Wang Y-P, Li X-T, Zhao X, Dong J and Zhang Q-H 2022 Dry-spun polyimide fibers with excellent thermal stability, intrinsic flame retardancy and ultralow smoke release *Chin. J. Polym. Sci.* **40** 1422–31
[16] Satoh R, Morinaga T and Sato T 2022 Novel dry spinning process of natural macromolecules for sustainable fiber material-1-proof of the concept using silk fibroin *Materials* **15** 4195
[17] Li T, Mao Z, Du J, Liu L and Wang B 2023 Shear-governed microstructural variation and evolution of PPTA in dry-jet-wet spinning process *Int. J. Mech. Sci.* **240** 107950
[18] Guizani C, Nieminen K, Rissanen M, Larkiala S, Hummel M and Sixta H 2020 New insights into the air gap conditioning effects during the dry-jet wet spinning of an ionic liquid-cellulose solution *Cellulose* **27** 4931–48
[19] Al Aiti M *et al* 2020 Dry-jet wet spinning of thermally stable lignin-textile grade polyacrylonitrile fibers

regenerated from chloride-based ionic liquids compounds *Materials* **13** 3687
[20] Mahalingam S and Edirisinghe M 2013 Forming of polymer nanofibers by a pressurised gyration process *Macromol. Rapid Commun.* **34** 1134–9
[21] Dai Y, Ahmed J, Delbusso A and Edirisinghe M 2022 Nozzle-pressurized gyration: a novel fiber manufacturing process *Macromol. Mater. Eng.* **307** 2270038
[22] Bhardwaj N and Kundu S C 2010 Electrospinning: a fascinating fiber fabrication technique *Biotechnol. Adv.* **28** 325–47
[23] Yarin A L, Koombhongse S and Reneker D H 2001 Bending instability in electrospinning of nanofibers *J. Appl. Phys.* **89** 3018–26
[24] Garg K and Bowlin G L 2011 Electrospinning jets and nanofibrous structures *Biomicrofluidics* **5** 013403
[25] Lin J, Wang X, Ding B, Yu J, Sun G and Wang M 2012 Biomimicry via Electrospinning *Crit. Rev. Solid State Mater. Sci.* **37** 94–114
[26] Li Y, Zhu J, Cheng H, Li G, Cho H, Jiang M, Gao Q and Zhang X 2021 Developments of advanced electrospinning techniques: a critical review *Adv. Mater. Technol.* **6** 2100410
[27] Teo W E and Ramakrishna S 2006 A review on electrospinning design and nanofibre assemblies *Nanotechnology* **17** R89–R106
[28] Holland C, Numata K, Rnjak-Kovacina J and Seib F P 2019 The biomedical use of silk: past, present future *Adv. Healthcare Mater.* **8** 1800465
[29] Heim M, Keerl D and Scheibel T 2009 Spider silk: from soluble protein to extraordinary fiber *Angew. Chem., Int. Ed.* **48** 3584–96
[30] Asakura T, Umemura K, Nakazawa Y, Hirose H, Higham J and Knight D 2007 Some observations on the structure and function of the spinning apparatus in the silkworm bombyx mori *Biomacromolecules* **8** 175–81
[31] Koeppel A and Holland C 2017 Progress and trends in artificial review silk spinning: a systematic review *ACS Biomater. Sci. Eng.* **3** 226–37
[32] Humenik M, Lang G and Scheibel T 2018 *Silk nanofibril self-assembly versus electrospinning Wiley Interdiscip. Rev.-Nanomed. Nanobiotechnol.* **10** e1509
[33] Andersson M, Johansson J and Rising A 2016 Silk spinning in silkworms and spiders *Int. J. Mol. Sci.* **17** 1290
[34] Kronqvist N *et al* 2014 Sequential pH-driven dimerization and stabilization of the N-terminal domain enables rapid spider silk formation *Nat. Commun.* **5** 3254
[35] Scheibel T 2004 Spider silks: recombinant synthesis, assembly, spinning, and engineering of synthetic proteins *Microb. Cell Factories* **3** 14
[36] Hinman M B, Jones J A and Lewis R V 2000 Synthetic spider silk: a modular fiber *Trends Biotechnol.* **18** 374–9
[37] Huemmerich D, Scheibel T, Vollrath F, Cohen S, Gat U and Ittah S 2004 Novel assembly properties of recombinant spider dragline silk proteins *Curr. Biol.* **14** 2070–4
[38] Rising A and Johansson J 2015 Toward spinning artificial spider silk *Nat. Chem. Biol.* **11** 309–15
[39] Gosline J M, Guerette P A, Ortlepp C S and Savage K N 1999 The mechanical design of spider silks: from fibroin sequence to mechanical function *J. Exp. Biol.* **202** 3295–303
[40] Rockwood D N, Preda R C, Yücel T, Wang X, Lovett M L and Kaplan D L 2011 Materials fabrication from Bombyx mori silk fibroin *Nat. Protocols* **6** 1612–31
[41] Carissimi G, Lozano-Pérez A A, Montalbán M G, Aznar-Cervantes S D, Cenis J L and Víllora G 2019 Revealing the influence of the degumming process in the properties of silk fibroin nanoparticles *Polymers* **11** 2045
[42] Feng Y F, Lin J, Niu L, Wang Y, Cheng Z, Sun X and Li M 2020 High molecular weight silk fibroin prepared by papain degumming *Polymers* **12** 2105
[43] Freddi G, Mossotti R and Innocenti R 2003 Degumming of silk fabric with several proteases *J. Biotechnol.* **106** 101–12
[44] Anand P, Pandey J P and Pandey D M 2021 Study on cocoonase, sericin, and degumming of silk cocoon: computational and experimental *J. Genet. Eng. Biotechnol.* **19** 32
[45] Wei W, Zhang Y, Zhao Y, Luo J, Shao H and Hu X 2011 Bio-inspired capillary dry spinning of regenerated silk fibroin aqueous solution *Mater. Sci. Eng.* C **31** 1602–8
[46] Jin Y, Zhang Y, Hang Y, Shao H and Hu X 2013 A simple process for dry spinning of regenerated silk fibroin aqueous solution *J. Mater. Res.* **28** 2897–902
[47] Peng Q, Shao H, Hu X and Zhang Y 2015 Role of humidity on the structures and properties of regenerated silk fibers *Prog. Nat. Sci.: Mater. Int.* **25** 430–6
[48] Luo J, Zhang L, Peng Q, Sun M, Zhang Y, Shao H and Hu X 2014 Tough silk fibers prepared in air using a biomimetic microfluidic chip *Int. J. Biol. Macromol.* **66** 319–24
[49] Li D, Jacobsen M M, Gyune Rim N, Backman D, Kaplan D L and Wong J Y 2017 Introducing biomimetic shear and ion gradients to microfluidic spinning improves silk fiber strength *Biofabrication* **9** 025025
[50] Magaz A N, Roberts A D, Faraji S, Nascimento T R L, Medeiros E S, Zhang W, Greenhalgh R D, Mautner A, Li X and Blaker J J 2018 Porous, aligned, and biomimetic fibers of regenerated silk fibroin produced by solution blow spinning *Biomacromolecules* **19** 4542–53
[51] Jin H-J and Kaplan D L 2003 Mechanism of silk processing in insects and spiders *Nature* **424** 1057–61
[52] Andersson M *et al* 2017 Biomimetic spinning of artificial spider silk from a chimeric minispidroin *Nat. Chem. Biol.* **13** 262–4
[53] Greco G, Francis J, Arndt T, Schmuck B, G. Bäcklund F, Barth A, Johansson J, M. Pugno N and Rising A 2020 Properties of biomimetic artificial spider silk fibers tuned by postspin bath incubation *Molecules* **25** 3248
[54] Schmuck B, Greco G, Bäcklund F G, Pugno N M, Johansson J and Rising A 2022 Impact of physio-chemical spinning conditions on the mechanical properties of biomimetic spider silk fibers *Commun. Mater.* **3** 83
[55] Arndt T *et al* 2022 Engineered spider silk proteins for biomimetic spinning of fibers with toughness equal to dragline silks *Adv. Funct. Mater.* **32** 2200986
[56] Heidebrecht A, Eisoldt L, Diehl J, Schmidt A, Geffers M, Lang G and Scheibel T 2015 Biomimetic fibers made of recombinant spidroins with the same toughness as natural spider silk *Adv. Mater.* **27** 2189–94
[57] Stengel D, Saric M, Johnson H R, Schiller T, Diehl J, Chalek K, Onofrei D, Scheibel T and Holland G P 2023 Tyrosine's unique role in the hierarchical assembly of recombinant spider silk proteins: from spinning dope to fibers *Biomacromolecules* **24** 1463–74
[58] Saric M, Eisoldt L, Döring V and Scheibel T 2021 Interplay of different major ampullate spidroins during assembly and implications for fiber mechanics *Adv. Mater.* **33** 2006499
[59] Saric M and Scheibel T 2023 Two-in-one spider silk protein with combined mechanical features in all-aqueous spun fibers *Biomacromolecules* **24** 1744–50
[60] Lu L, Fan S, Niu Q, Peng Q, Geng L, Yang G, Shao H, Hsiao B S and Zhang Y 2019 Strong silk fibers containing cellulose nanofibers generated by a bioinspired microfluidic chip *ACS Sustain. Chem. Eng.* **7** 14765–74
[61] Jao D, Hu X and Beachley V 2021 Bioinspired silk fiber spinning system via automated track-drawing *ACS Appl. Bio Mater.* **4** 8192–204
[62] Vendrely C and Scheibel T 2007 Biotechnological production of spider-silk proteins enables new applications *Macromol. Biosci.* **7** 401–9
[63] Ricard-Blum S 2011 The collagen family *Cold Spring Harb. Perspect. Biol.* **3** a004978
[64] Gelse K, Poschl E and Aigner T 2003 Collagens—structure, function, and biosynthesis *Adv. Drug Deliv. Rev.* **55** 1531–46
[65] Revell C K, Jensen O E, Shearer T, Lu Y, Holmes D F and Kadler K E 2021 Collagen fibril assembly: new approaches to unanswered questions *Matrix Biol. Plus* **12** 100079

[66] Bazrafshan Z and Stylios G K 2019 Spinnability of collagen as a biomimetic material: a review *Int. J. Biol. Macromol.* **129** 693–705
[67] Sizeland K H *et al* 2018 Nanostructure of electrospun collagen: do electrospun collagen fibers form native structures? *Materialia* **3** 90–96
[68] Haynl C, Hofmann E, Pawar K, Förster S and Scheibel T 2016 Microfluidics-produced collagen fibers show extraordinary mechanical properties *Nano Lett.* **16** 5917–22
[69] Hepworth D G and Smith J P 2002 The mechanical properties of composites manufactured from tendon fibres and pearl glue (animal glue) *Composites* A **33** 797–803
[70] Gosline J, Lillie M, Carrington E, Guerette P, Ortlepp C and Savage K 2002 Elastic proteins: biological roles and mechanical properties *Phil. Trans. R. Soc.* B **357** 121–32
[71] Dasgupta A *et al* 2021 Comprehensive collagen crosslinking comparison of microfluidic wet-extruded microfibers for bioactive surgical suture development *Acta Biomater.* **128** 186–200
[72] Tronci G, Kanuparti R S, Arafat M T, Yin J, Wood D J and Russell S J 2015 Wet-spinnability and crosslinked fibre properties of two collagen polypeptides with varied molecular weight *Int. J. Biol. Macromol.* **81** 112–20
[73] Tonndorf R, Gossla E, Aibibu D, Lindner M, Gelinsky M and Cherif C 2019 Wet spinning and riboflavin crosslinking of collagen type I/III filaments *Biomed. Mater.* **14** 039501
[74] Yaari A, Schilt Y, Tamburu C, Raviv U and Shoseyov O 2016 Wet spinning and drawing of human recombinant collagen *ACS Biomater. Sci. Eng.* **2** 349–60
[75] Koeck K S, Salehi S, Humenik M and Scheibel T 2022 Processing of continuous non-crosslinked collagen fibers for microtissue formation at the muscle-tendon interface *Adv. Funct. Mater.* **32** 2112238
[76] Kadler K E, Holmes D F, Trotter J A and Chapman J A 1996 Collagen fibril formation *Biochem. J.* **316** 1–11
[77] Shields K J, Beckman M J, Bowlin G L and Wayne J S 2004 Mechanical properties and cellular proliferation of electrospun collagen type II *Tissue Eng.* **10** 1510–7
[78] Wang L *et al* 2022 Large-scalable polar bear hair-like cellular hollow fibers with excellent thermal insulation and ductility *J. Appl. Polym. Sci.* **139** e53018
[79] Zhao Y and Fang F 2022 A biomimetic textile with self-assembled hierarchical porous fibers for thermal insulation *ACS Appl. Mater. Interfaces* **14** 25851–60
[80] Chen Q, Fan J and Sarkar M 2010 Biomimetics of plant structure in knitted fabrics to improve the liquid water transport properties *Text. Res. J.* **80** 568–76
[81] Wang X, Huang Z, Miao D, Zhao J, Yu J and Ding B 2019 Biomimetic fibrous murray membranes with ultrafast water transport and evaporation for smart moisture-wicking fabrics *ACS Nano* **13** 1060–70
[82] Miao D *et al* 2021 A biomimetic transpiration textile for highly efficient personal drying and cooling *Adv. Funct. Mater.* **31** 2008705
[83] Ureña-Benavides E E and Kitchens C L 2012 Cellulose nanocrystal reinforced alginate fibers—biomimicry meets polymer processing *Mol. Cryst. Liq. Cryst.* **556** 275–87
[84] Podgórski A, Bałazy A and Gradon L 2006 Application of nanofibers to improve the filtration efficiency of the most penetrating aerosol particles in fibrous filters *Chem. Eng. Sci.* **61** 6804–15
[85] Liu H, Liu L, Yu J, Yin X and Ding B 2020 High-efficiency and super-breathable air filters based on biomimetic ultrathin nanofiber networks *Compos. Commun.* **22** 100493
[86] Liu H, Zhang S, Liu L, Yu J and Ding B 2020 High-performance filters from biomimetic wet-adhesive nanoarchitectured networks *J. Mater. Chem.* A **8** 18955–62
[87] Burgard M, Weiss D, Kreger K, Schmalz H, Agarwal S, Schmidt H-W and Greiner A 2019 Mesostructured nonwovens with penguin downy feather-like morphology—top-down combined with bottom-up *Adv. Funct. Mater.* **29** 1903166
[88] Guan Q-F *et al* 2021 Biomimetic design and mass production of sustainable multiscale cellulose fibers-based hierarchical filter materials for protective clothing *Adv. Mater. Technol.* **6** 2100193
[89] Li H *et al* 2022 Biomimetic on-chip filtration enabled by direct micro-3D printing on membrane *Sci. Rep.* **12** 1–9
[90] Ling S *et al* 2017 Design and function of biomimetic multilayer water purification membranes *Sci. Adv.* **3** e1601939
[91] Homaeigohar S, Disci-Zayed D, Dai T and Elbahri M 2013 Biofunctionalized nanofibrous membranes mimicking carnivorous plants *Bioinspired Biomim. Nanobiomaterials* **2** 186–93
[92] Jia L *et al* 2019 Microfluidic fabrication of biomimetic helical hydrogel microfibers for blood-vessel-on-a-chip applications *Adv. Healthcare Mater.* **8** 1900435
[93] Xie R *et al* 2021 Composable microfluidic spinning platforms for facile production of biomimetic perfusable hydrogel microtubes *Nat. Protocols* **16** 937–64
[94] Xie R, Korolj A, Liu C, Song X, Lu R X Z, Zhang B, Ramachandran A, Liang Q and Radisic M 2020 h-FIBER: microfluidic topographical hollow fiber for studies of glomerular filtration barrier *ACS Cent. Sci.* **6** 903–12
[95] Zuo Y, He X, Yang Y, Wei D, Sun J, Zhong M, Xie R, Fan H and Zhang X 2016 Microfluidic-based generation of functional microfibers for biomimetic complex tissue construction *Acta Biomater.* **38** 153–62
[96] Zhou F-L, McHugh D J, Li Z, Gough J E, Williams G R and Parker G J M 2021 Coaxial electrospun biomimetic copolymer fibres for application in diffusion magnetic resonance imaging *Bioinsp. Biomim.* **16** 046016
[97] Liewald D, Miller R, Logothetis N, Wagner H-J and Schüz A 2014 Distribution of axon diameters in cortical white matter: an electron-microscopic study on three human brains and a macaque *Biol. Cybern.* **108** 541–57
[98] Lowery J L, Datta N and Rutledge G C 2010 Effect of fiber diameter, pore size and seeding method on growth of human dermal fibroblasts in electrospun poly(3-caprolactone) fibrous mats *Biomaterials* **31** 491–504
[99] Sisson K *et al* 2010 Fiber diameters control osteoblastic cell migration and differentiationin electrospun gelatin *J. Biomed. Mater. Res.* **94A** 1312–20
[100] Heseltine P L, Bayram C, Gultekinoglu M, Homer-Vanniasinkam S, Ulubayram K and Edirisinghe M 2022 Facile one-pot method for all aqueous green formation of biocompatible silk fibroin-poly(ethylene oxide) fibers for use in tissue engineering *ACS Biomater. Sci. Eng.* **8** 1290–300
[101] Qi P, Zhou Y, Wang D, He Z and Li Z 2015 A new collagen solution with high concentration and collagen native structure perfectly preserved *RSC Adv.* **5** 87180–6
[102] Yang L, Fitié C F C, van der Werf K O, Bennink M L, Dijkstra P J and Feijen J 2008 Mechanical properties of single electrospun collagen type I fibers *Biomaterials* **29** 955–62
[103] Wang S, Banerjee A, Matarlo B, Arinzeh T L, Ophir Z, Jaffe M and Collins G 2012 Structure and morphology of electrospun collagen blends *Bioinspired Biomim. Nanobiomaterials* **1** 202–13
[104] Pant H R, Risal P, Park C H, Tijing L D, Jeong Y J and Kim C S 2013 Core–shell structured electrospun biomimetic composite nanofibers of calcium lactate-nylon-6 for tissue engineering *Biochem. Eng. J.* **221** 90–98
[105] Park K E, Kang H K, Lee S J, Min B-M and Park W H 2006 Biomimetic nanofibrous Scaffolds: preparation and characterization of PGA/Chitin blend nanofibers *Biomacromolecules* **7** 635–43
[106] Zhixiao L *et al* 2021 Epidermal stem cells maintain stemness via a biomimetic micro/nanofiber scaffold that

promotes wound healing by activating the Notch signaling pathway *Stem Cell Res. Ther.* **12** 341
[107] Narayanan N, Jiang C, Wang C, Uzunalli G, Whittern N, Chen D, Jones O G, Kuang S and Deng M 2020 Harnessing fiber diameter-dependent effects of myoblasts toward biomimetic scaffold-based skeletal muscle regeneration *Front. Bioeng. Biotechnol.* **8** 203
[108] Nelson M T, Short A, Cole S L, Gross A C, Winter J, Eubank T D and Lannutti J J 2014 Preferential, enhanced breast cancer cell migration on biomimetic electrospun nanofiber 'cell highways' *BMC Cancer* **14** 825
[109] He C *et al* 2022 Biomimetic asymmetric composite dressing by electrospinning with aligned nanofibrous and micropatterned structures for severe burn wound healing *ACS Appl. Mater. Interfaces* **14** 32799–812
[110] Hu Q, Wu C and Zhang H 2020 Preparation and optimization of a biomimetic triple-layered vascular scaffold based on coaxial electrospinning *Appl. Biochem. Biotechnol.* **190** 1106–23
[111] Shao W, He J, Han Q, Sang F, Wang Q, Chen L, Cui S and Ding B 2016 A biomimetic multilayer nanofiber fabric fabricated by electrospinning and textile technology from polylactic acid and Tussah silk fibroin as a scaffold for bone tissue engineering *Modelling Simul. Mater. Sci. Eng.* C **67** 599–610
[112] Tang J, Wu C, Chen S, Qiao Z, Borovskikh P, Shchegolkov A, Chen L, Wei D, Sun J and Fan H 2020 Combining electrospinning and electrospraying to prepare a biomimetic neural Scaffold with synergistic cues of topography and electrotransduction *ACS Appl. Bio Mater.* **3** 5148–59
[113] Amarakoon M, Alenezi H, Homer-Vanniasinkam S and Edirisinghe M 2022 Environmental impact of polymer fiber manufacture *Macromol. Mater. Eng.* **307** 2200356
[114] Dai Y, Ahmed J and Edirisinghe M 2023 Pressurized gyration: fundamentals, advancements, and future *Macromol. Mater. Eng.* **24** 2300033
[115] Müller F, Jokisch S, Bargel H and Scheibel T 2020 Centrifugal electrospinning enables the production of meshes of ultrathin polymer fibers *ACS Appl. Polym. Mater.* **2** 4360–7